Micro-electrical discharge machining of large aspect ratio blind micro-holes using a novel self-flushing technique

Zhixiang Zou [1, 2] · Zhijian Huang [2] · Kangcheung Chan [3] · Taiman Yue [3] ·Zhongning Guo [2] · Jiangwen Liu [2,*]

[1] School of Mechatronic Engineering, Guangdong Polytechnic Normal University, Guangzhou, Guangdong, 510665, PR China

[2] State Key Laboratory of Precision Electronic Manufacturing Technology and Equipment, Guangdong University of Technology, Guangzhou 510006, PR China

[3] State Key Laboratory of Ultra-precision Machining Technology, Department of Industrial and Systems Engineering, The Hong Kong Polytechnic University, Hong Kong, China

*Corresponding author: Jiangwen Liu.

Email: fejwliu@scut.edu.cn

ABSTRACT

Due to the debris accumulates in the central areas of the inter-electrode gap (IEG) and being difficult to evacuate in the micro-electrical discharge machining (micro-EDM) process, achieving a large aspect ratio (AR) for blind micro-holes remains a significant challenge. Based on our previous research on debris secondary flow distribution theory in micro-EDM, we propose a novel self-flushing technique using a center-slotted tool electrode to enhance debris evacuation in the central regions of the IEG. A simulation model was developed to analyze the motion and distributions of debris under the self-flushing

technique operation. A simulation model was developed to analyze the motion and distribution of debris under the operation of the self-flushing technique. The results indicated that a secondary flow effect occurred within the IEG, concentrating most debris at the center. In comparison to the conventional solid cylindrical tool approach, the debris evacuated through the central slot pathway with the self-flushing effect. Experiments were undertaken to validate the model and the experimental results were well matched with the simulation. Furthermore, the machining efficiency was improved by 73.1 % using the self-flushing technique. The slot position and width of the slotted tool electrode and speed of rotation was also shown an important contribution to the effectiveness of self-flushing. A blind micro-hole with an impressive AR of 27.42 (corresponding to a depth of 5.41 mm and an entrance diameter of 197.3 μm) was successfully drilled. This represents the highest AR reported to date for Ti6Al4V alloy using micro-EDM. This novel self-flushing technique is innovatively solved the challenge of difficulty in exhausting debris that accumulated in the center IEG due to the secondary flow effect. It is concluded that the novel self-flushing technique is highly transferrable to process a large AR blind micro-hole on Ti6Al4V alloys.

Keyword: Micro-EDM; Large AR micro-hole; Secondary flow; Self-flushing technique; Center slotted tool electrode

1 Introduction

In recent years, a larger AR (depth-to-diameter ratio) ≥ 5 micro-holes was growing in numerous commercial applications [1]. Tiwary et al. [2] stated that the fabrication of large AR micro-holes as among the most common operations in the manufacturing of many engineering parts. However, such parts demand high strength-to-weight ratios as well as good corrosion resistance at extreme temperatures

and pressures, and thus they are frequently fabricated with materials such as Ti6Al4V alloys. In general, the common methods of micro-hole manufacture include mechanical micro drilling, laser drilling, micro-electrochemical machining (micro-ECM) and micro-EDM [3]. Routio et al. [4] reported that conventional mechanical micro drilling was usually constrained by workpiece material properties such as strength and hardness, etc. Nasrollahi et al. [5] stated that laser drilling resulted in holes with large tapers and severe material splatter, as well as a limited achievable micro-hole AR. As for micro-ECM, it has significant advantages for processing difficult-to-cut metal materials [6]. Chen et al. [7] stated that the ECM was normally affected by the flow fields, electric fields, and chemical corrosion properties. Consequently, the processing stability would be probably be affected [8]. Among these methods, the micro-EDM can machine almost all conductive material regardless of the hardness and strength properties of the workpiece materials [9-10]. Thus, micro-EDM is frequently employed to manufacture micro-hole in the hard-to-process material [11].

However, in micro-EDM, the flushing of debris and bubbles from the IEG becomes challenging when increasing the drilling depth of blind micro-holes. Consequently, frequent abnormal discharges and short circuits occur, causing low machining efficiency and extensive tool electrode wear, especially limiting the AR of blind micro-holes[12]. Wang et al. [13-14] proposed a three-dimensional flow field model involving liquid, gas, and solid phases within the inter-electrode gap (IEG) during EDM drilling. They reported that bubble expansion serves as the primary mechanism for expelling bubbles from the machining gap. A significant amount of debris is carried out of the IEG along with the expanding bubbles. However, this expelling effect weakens when the bubbles reach the side gap (i.e., the micro-hole wall), where bubbles may even block the side gap. This blockage reduces or entirely stops the flow of working fluid within the IEG, causing debris to accumulate in the bottom gap. Consequently, frequent short

67 circuits or arc discharges occur [15]. To overcome this issue, researchers focused on increasing the debris
68 and bubbles removal using various approaches, such as ultrasound assisted, tool electrode planetary
69 movement, flushing and shaped tool electrodes, etc. Zhao et al. [16] observed that ultrasonic vibration
70 assistance can improve the liquid flow behavior substantially, and hence decrease the debris gathering in
71 the IEG, leading to increasing the machining efficiency and the micro-hole AR size. In addition, Li et al.
72 [17] employed an ultrasonic circular round vibrating electrode to improve the circulating liquid medium
73 and debris removal in the IEG, resulting in an increased micro-hole machining performance. Despite the
74 fact that ultrasonic vibration assistance can improve the debris removal, this usually caused the micro-
75 EDM process to be unstable or even unattainable under the ultra-small energy conditions [18-19].
76 Furthermore, Bamberg et al. [20] offset the electrodes to a specific value for providing planetary motion.
77 In this manner, the debris is easily to remove from the IEG zone, resulting in increased flushing and
78 reduction of the tool electrode wear. Accordingly, Yu et al. [21] combined planetary motion and the
79 ultrasonic vibrations to produce an unevenly distribution gap for debris and/or gas bubble to exit from
80 the IEG, and as a consequence, both the processing efficiency and micro-hole AR size increased.
81 On the other hand, it should be noted that there is no useful self-flushing strategy besides the solid
82 tool rotation and bubble movement under the blind micro-hole processing in traditional micro-EDM [22].
83 In spite of the fact that the rotary tubular tool electrode can provide effective flushing and avoid the
84 debris accumulating in the IEG, residual is formed in the micro-hole bottom. More recently, Li et al. [23]
85 used the mist deionized water jet in drilling micro-holes, which lead to increasing the debris removal and
86 a deeper micro-hole was achieved. Nonetheless, developing the mist deionized water jet system and
87 controlling the mist flow rate is burdensome and an additional complication. Furthermore, as the
88 manufacturing tool electrode technique advanced, shaped tool electrodes (i.e. helical electrode, notch

electrode, incline slot electrode and inclined through-hole electrode) are widely used, and which play a critically role in the prevention of debris accumulations in the IEG. Plaza et al. [24] applied helical-shaped electrodes and micro-hole diameter of 661 μm, and an AR of 10 was drilled. Kumar et al. [10] observed that the notch tool electrode offers a channel for the debris take can easily be cleaned away from the IEG, and thus, a high machining efficiency with relatively low tool electrode wear rate was achieved. Further, Kumar et al. [25] proposed a tool electrode with inclined micro-channels to help remove debris from the IEG. In comparison to a solid cylindrical tool electrode, the AR value is increased by 300%. Moreover, Kumar et al. [26] drilled the inclined through micro-holes into the solid tool and found the debris and bubbles could exit from the micro slot through the hole. As a consequence, a large AR micro-hole (i.e., AR of 12.25) was successfully fabricated. Nevertheless, it should be noted that these structures of helical and incline a slot on the tool electrode surface were usually damaged due to the inevitable tool electrode wear that occurred. As a result, the stable and continuous debris removal of such shaped tool electrodes will not be maintained, which restricts the AR of micro-hole. Moreover, fabrication of the inclined through hole on the tool electrode surface is usually restricted by the tool diameter (e.g., drilling inclined micro-holes on tool electrodes with diameters of less than 200 μm is challenging). In addition, according to Kumar et al. [27], when fabricating a large AR micro-hole, drilling multiple pathway inclined holes into the solid cylindrical tool electrode is required and needs extra attention. Consequently, although these shaped electrodes can provide a better debris removal capability, it is challenging to manufacture shaped tool electrodes with large aspect ratios for processing blind micro-holes (with diameters < 200 μm). As a result, further increasing the AR of blind micro-holes is still a big challenge.

As discussed earlier, most of literature focuses on how to remove debris out from the IEG, while

only a few papers report how the debris is distributed in the IEG. Ichikawa et al. [18] found that debris are hard to cleared out of the center region of the IEG. Ekmekci et al. [27] reported that the debris accumulates in a conical formation at the micro-hole's bottom center region. That is to say, most of debris is distributed in the center region of IEG under the tool rotation condition. Interestingly, this distribution of debris is similar to the well-known Einstein's tea leaf paradox. i.e., secondary flow theory. Einstein [28] discovered that when tea was stirred in a cup with chopsticks, the leaves gathered in the bottom center of the cup. Since the pressure at the edge of the cup is larger than at the center of cup, producing a secondary flow effect, the tea leaves are moving towards the center area. Most recently, in our previous work, Zou et al. [29] reported for the first time that the debris accumulated in the central area of the IEG under the secondary flow effect in the micro-EDM. In general, the discharge channel will produce a greater pressure, disturbing the accumulation of debris in the IEG and/or causing the debris and bubbles to escape from the side gap. However, Ekmekci et al. [27] reported, in the pulse-off time, the channel pressure is drastically decreased, leading to the pressure at the edge of the micro-hole being larger than in the central area. Consequently, this pressure difference forces previously discharged debris back into the IEG's central area. Also, this changed pressure may further strengthen the secondary flow effect in the pulse-off time. There is no doubt that the accumulation of debris in the central IEG and the difficulty of removing is one of the main reasons for the frequent abnormal discharges, resulting in a reduction of the AR.

Inspired by this, a new self-flushing technique (i.e., center slotted tool electrode) based on the secondary flow theory is firstly proposed to improve the removal of the debris accumulating in the central areas of IEG. Furthermore, a simulation model was conducted to analyze the motion and distributions of debris in the IEG to understand its mechanisms. Experiments were also further performed to evaluate the

effectivity of this new self-flushing technique in increasing the AR of blind micro-holes using micro-EDM.

2 Method description of the novel self-flushing technique

According to Einstein [28], tea leaves movement towards the center of the cup bottom owing to the secondary flow effect (i.e., the tea paradox phenomenon). However, the rotation of the tool electrode rotates the working fluid in the micro-EDM. Clearly, the motion and distribution of debris are quite similar to the tea leaves (Fig. 1(a)). Furthermore, Fig. 1(b) indicates that the secondary flow effect forces the debris to gather in the micro-hole bottom center [29]. As compared to solid cylindrical tool electrodes, center slotted tool electrodes help to provide a self-flushing effect under the tool electrode rotation condition. Also, the center slotted tool electrode (i.e., self-flushing electrode) provides a central slot pathway for the debris evacuation. It is envisaged that the self-flushing electrode is not only able to produce a self-flushing effect, but also removes debris from the IEG through central slot pathway (Fig. 1(c)). Furthermore, debris accumulation in the center of the IEG caused by the secondary flow effect would be avoided. That is to say, the problem of debris accumulating in the center IEG and being difficult to exhaust because of the secondary flow effect can be overcome. Consequently, the self-flushing effect can enable sufficient de-ionization between IEG in the subsequent pulse-on time. On the other hand, compared to the helical and inclined slot on the tool surface, since the debris removal pathway is inside the center slotted tool, the center slotted pathway is minimally worn (Fig. 1(c)). Accordingly, combining the action of the secondary flow effect, this proposed tool electrode can provide a stable and continuous debris exhaust in the micro-EDM. However, it should be noted that the inefficient debris evacuation causes a severe arcing and short circuits in the IEG, resulted in an increasing in tool electrode wear,

lowing machining efficiency, especially limiting the AR of micro-holes [12]. As a result, the proposed self-flushing tool electrode has a better potential for processing large AR blind micro-hole than that of the conventional solid cylindrical tool. To further understand the self-flushing technique, more detailed theoretical and experimental investigations will be examined and the results are presented in the subsequent sections.

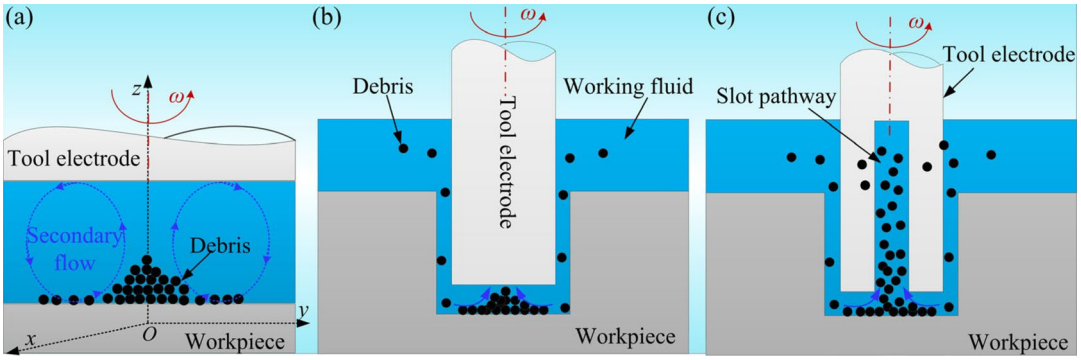

Fig. 1. **(a)** Schematic of secondary flow under the IEG. The evacuation of debris **(b)** under the solid cylindrical, and **(c)** under the center slotted tool electrode with novel self-flushing effect.

3 Theoretical analyses of novel self-flushing technique

3.1 Model development

As discussed earlier, Li et al. [22] stated that there is no effective self-flushing approach except the bubble movement and tool rotation in the conventional blind hole drilling of EDM with a solid tool. Moreover, without additional flushing effect, a part of the bubbles is blocked in the hole wall, which affects the debris removal [13]. On the other hand, despite the flushing effect produced by the tool rotation, bubbles and debris can be removed from the side wall gap. However, it should be noted that when no additional flushing effect, resulting in a part of the debris accumulating in the IEG center and being very difficult to remove [18,27]. Due to the debris is always conductive as a byproduct of metal materials, thus the accumulation of debris in the central IEG and the difficulty of removing is one of the

main reasons for the frequent abnormal discharges, leading to a poor machining performance [15]. Thus, a model was developed for analyzing the potential of the proposed novel self-flushing technique to solve the debris accumulation in the IEG center difficult to be removed. Since the EDM process is complex and bubbles have a significant effect on debris removal, the debris and bubbles observed at the hole exit using a high-speed camera in conjunction with the simulation results are further investigated in the subsequent experimental validation. As a consequence, the model was simplified and analyzed the movement and distribution of debris in the IEG. Other assumptions are: (1) no influence of bubbles generation and the fluid is incompressible, (2) tool electrode wear and workpiece materials removal are not considered, and (3) debris are from the workpiece material (Ti6Al4V), and debris are initially evenly and static distributed in the IEG. Fig. 2 shows the geometry established in the 3D model in *ANSYS FLUENT*. It consists of the working liquid (kerosene), the tool electrode (tungsten), and the workpiece (Ti6Al4V).

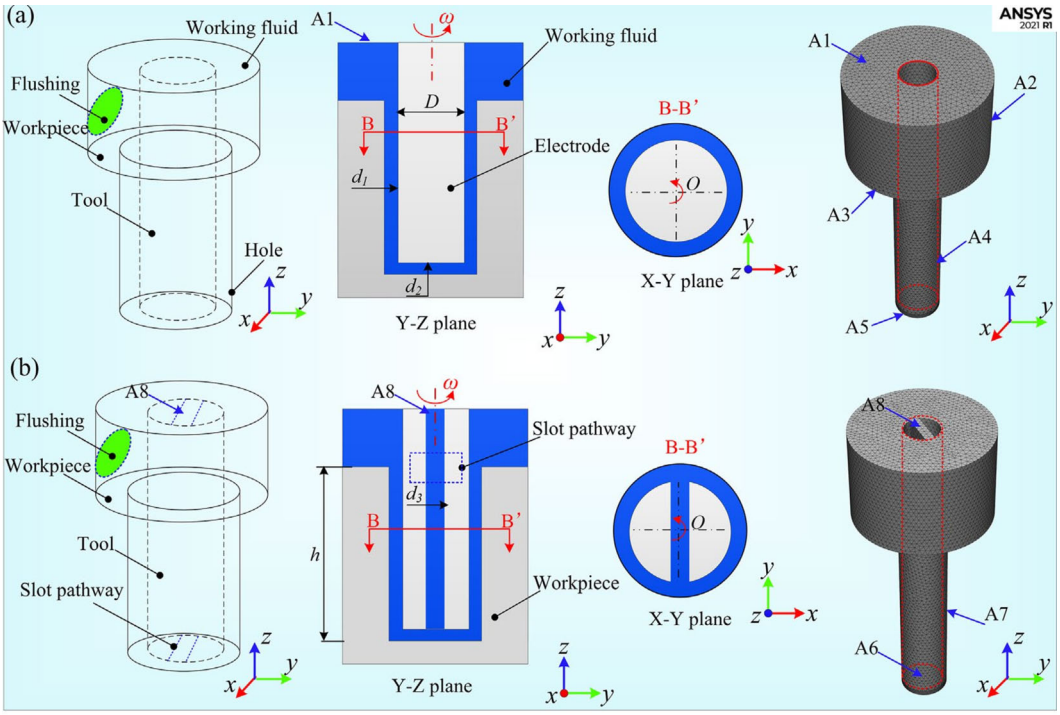

Fig. 2. 3D geometric model for micro-hole processing using **(a)** solid cylindrical tool electrode, and **(b)**

center slotted tool electrode.

Mastud et al. [30] stated the debris shape produced by the micro-EDM is spherical and the size is normally less than 1 μm. Thus, prior to the simulation process, the debris particles were collected and analyzed. SEM was applied to observe the debris particles and the its size distribution was measured using a particle size analyzer. It is can be observed from Fig. 3, the debris are spherical, with an average size of 488 nm. Accordingly, the debris particles are a spherical, with a diameter of 500 nm, in the simulation process. Since this work investigated the debris and flow field in blind micro-holes with large AR, thus the depth of the micro-holes was set to be 1000 μm and the inlet diameter to be 190 μm in the numerical modeling. Furthermore, Table 1 listed the simulation parameter values and boundaries in the simulation.

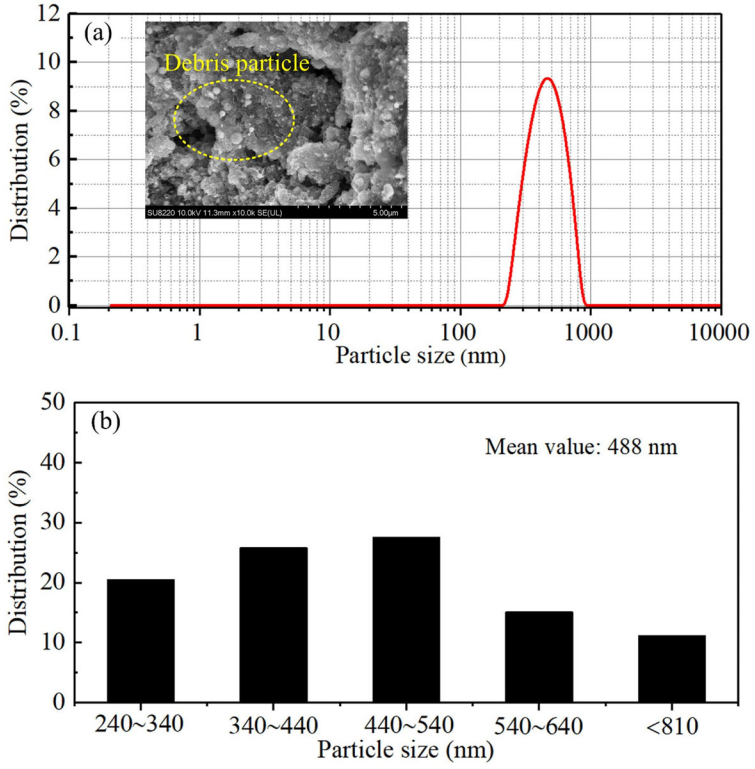

Fig. 3. The size distribution of debris particle.

202 **Table 1.** Parameters and boundaries for the simulation model.

Item	Value	Unit
Tool electrode diameter (D)	150	μm
Spindle speed	500	rpm
Side gap /d_1	20	μm
Machining gap /d_2	20	μm
Slot width /d_3	40	μm
Flushing port diameter	2	mm
Flushing velocity	2	m/s
Condition of boundaries	Condition of boundaries	Value
Outlet	A1, A8	P=0 Pa
Workpiece-fluid interface	A3	No slip
Wall	A2, A5, A7	No slip
Tool electrode-fluid interface	A4, A6	n=500 rpm

203 The equations for conservation of momentum and mass for the working liquid are given:

204 $$\rho\frac{\partial u}{\partial t}+\rho(u\cdot\nabla)u=\nabla\cdot\left[-PI+\mu\left(\nabla u+(\nabla u)^{T}\right)\right]+F \tag{1}$$

205 $$\frac{\partial \rho}{\partial t}+\nabla\cdot(\rho u)=0 \tag{2}$$

206 where u is a working liquid speed, ρ is a working liquid density, μ is is a working liquid dynamical
207 viscosity, p is a working liquid pressure, T is an absolutely temperature (K), F is the volume forces (N),
208 and I is the identification matrices. Moreover, debris particles tracking formulates the problem using
209 Lagrange's equation and then solves it taking Newton's second law of movement. Thus, the secondary
210 motion equation is used to calculate the location of the debris particles:

211 $$\frac{dq}{dt}=v \tag{3}$$

212 $$\frac{d}{dt}(m_p v)=F_t \tag{4}$$

213 where the q is the location of debris particles, v is the velocity of debris particles, and m_p is the mass

of debris particles. F_t is the total force of debris particles, and thus the fluid drag force F_D is the working liquid forces on the debris surface and calculated by:

$$F_D = \frac{1}{\tau_p} m_p \left(u - v\right) \tag{5}$$

where τ_p is a responding time of the particles, and u is the fluid velocity. The graviton force on the debris particles in solution is assumed to be:

$$F_g = m_p g \frac{\left(\rho_p - \rho_z\right)}{\rho_p} \tag{6}$$

where ρ_p is the particles density, ρ_z is the fluid density, and g is gravitational acceleration vector. Note that, when there is a differential speed of the liquid surrounding the debris particle, the Saffman forces $F_{saffman}$ can be written as:

$$F_{saffman} = 1.61 d_p^2 \left(\rho\mu\right)^{\frac{1}{2}} \left(u - v\right) \left|\frac{\partial u}{\partial l}\right|^{\frac{1}{2}} \tag{7}$$

where d_p is the diameter of the debris particle, $\partial u/\partial l$ is the fluid velocity gradient. When there is a pressure difference in the fluid around the debris particles. Thus, the pressure gradient F_p can be expressed as:

$$F_p = -\frac{\pi d_p^2}{6} \frac{\partial p}{\partial l} \tag{8}$$

where $\partial p/\partial l$ is the fluid pressure gradient. Thus, equation of motion of a particle in the fluid can be expressed as:

$$\frac{d}{dt}\left(m_p v\right) = F_D + F_g + F_{saff} + F_p \tag{9}$$

3.2 The distribution characteristic of flow and pressure field distribution

Fig. 4 compares the flow field distribution in the different tool electrodes. It can be observed that a high-flow field velocity area (red) is formed at the edge of the IEG, and a low-flow velocity area (blue)

is formed at the center of the IEG (Fig. 4(a)). Obviously, it indicates that the velocity of the fluid field increased gradually as distance from the micro-hole bottom center, which is very consistent with the well-known tea leaf paradox (secondary flow effect). It should be noted that there is a zero-flow field velocity at the workpiece wall due to this surface being a no-slip boundary. On the other hand, in the IEG (*YZ* plane), the ingress of clean fluid is through the side gaps, and the egress of the contaminated fluid is through the central slot pathway of the center slotted tool electrode (i.e., self-flushing effect) (Fig. 4(b)), which has significant difference with that of solid cylindrical electrode (Fig. 4(a)). Based on the secondary fluid effect, a self-flushing effect is formed in the center slotted tool electrode. Its primary function is to remove debris particles from the center area of the IEG and simultaneously introduce fresh working fluid into the IEG. This also means that a continuous circulation of working fluid is developed in the IEG. Thus, it is envisaged that the transport of debris through such central slot pathway would be of benefit in minimizing abnormal discharges in the IEG.

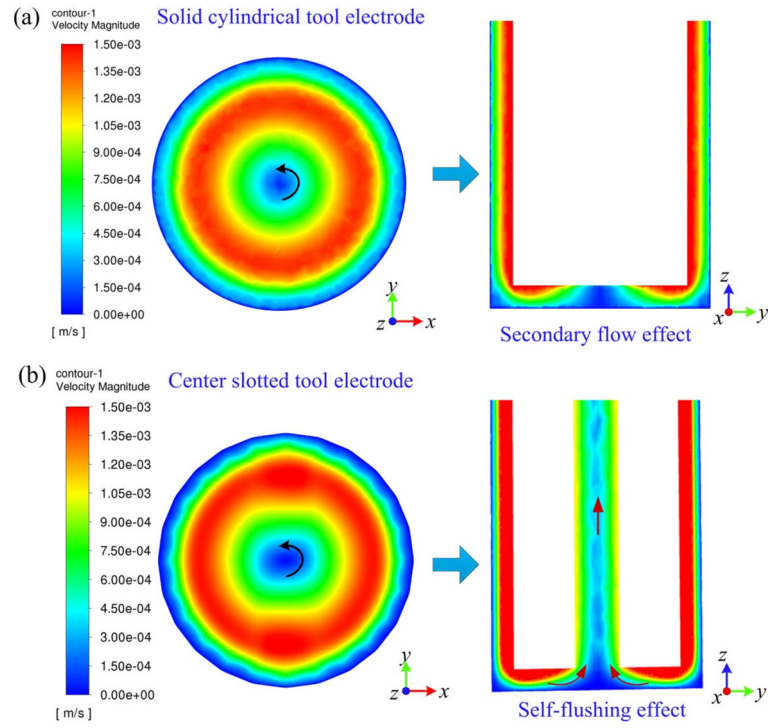

Fig. 4. The flow field distribution in (a) the solid cylindrical, and (b) the center slotted tool electrode.

Fig. 5 illustrates the pressure distributions superimposed with debris traces for the different tool electrodes. Both debris traces indicate that debris migrates from the bottom edge of the hole toward its central areas. This can be explained as follows: although the structure of the center-slotted electrode differs significantly from the conventional cylindrical electrode, the secondary flow effect still develops. During the discharge process (i.e., pulse-on time), high temperature and pressure are generated in the IEG, effectively removing debris from the gap. However, during the pulse-off time, the discharge channel pressure decreases sharply, causing the pressure at the hole's edge to become greater than that in the central area. This pressure difference forces the debris back into the central region of the IEG, as also reported by Ekmekci et al. [27]. This combined effect of pressure change and secondary flow leads to the dynamic accumulation of debris in the central area, making it difficult to evacuate. Consequently, with the solid cylindrical tool electrode (Fig. 5(a)), debris tends to accumulate in the central region, resulting in frequent abnormal discharges. In contrast, the proposed center-slotted pathway serves as a pressure relief port during both pulse-on and pulse-off times, facilitating the effective removal of debris from the IEG.

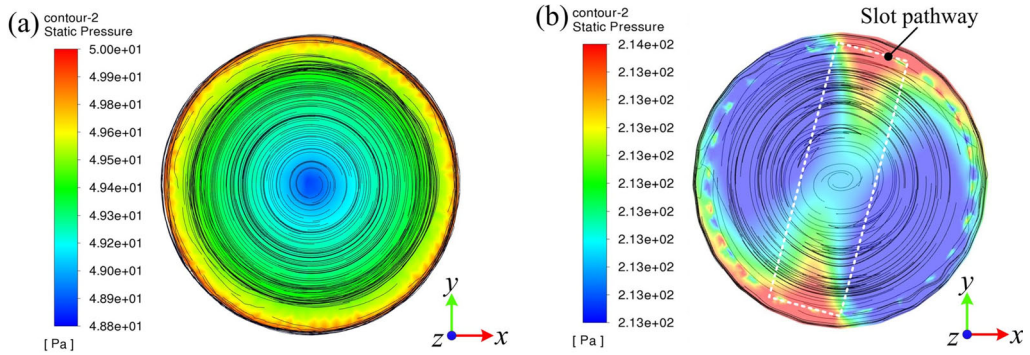

Fig. 5. The pressure distributions superposed with debris traces: (a) the solid cylindrical tool, and (b) the center slotted tool.

3.3 The distribution and movement characteristic of debris particles

To further investigate the relationship between the center-slotted tool and the debris distribution in the IEG, the results from 0.5 s to 1.5 s were analyzed to study the distribution and movement of debris particles. As observed, with the solid cylindrical tool, at 0.5 s, most of the debris is concentrated at the bottom of the IEG, while a small portion moves upward through the side gap (Fig. 6(a)). At later stages, the majority of the debris migrates toward the central area of the IEG, where it accumulates (Figs. 6(b) and 6(c)). As previously discussed, the discharge channel generates high pressure during the pulse-on time, which drives the debris to exit the IEG through the side gap. However, during the pulse-off time, the channel pressure decreases drastically, causing the pressure at the hole's edge to become greater than that at the center. According to Ekmekci et al. [27], this pressure change forces the previously discharged debris to return to the central region of the IEG. Similarly, Ichikawa et al. [18] reported that debris is difficult to clear from the central region of the IEG. Moreover, the secondary flow effect tends to accumulate debris particles in the central area of the IEG. It is hypothesized that the accumulation of debris in this central area increases the frequency of unusual discharges, which ultimately limits the achievable AR.

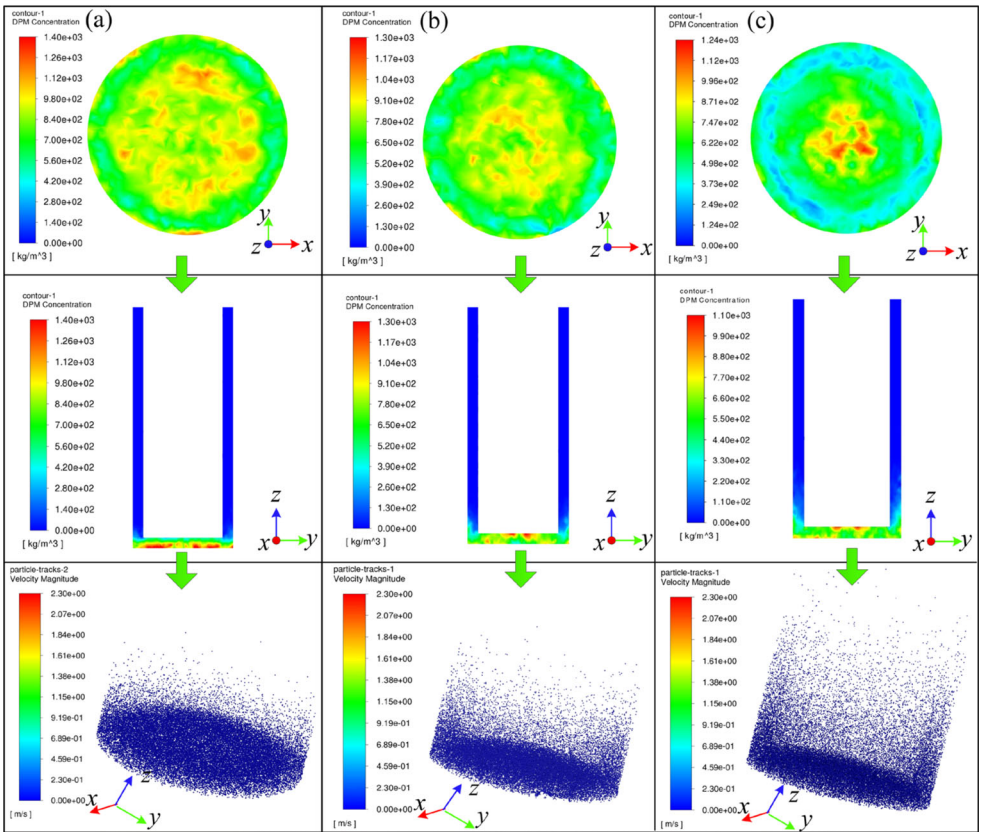

Fig. 6. The debris distribution in the solid cylindrical tool electrode with different times: **(a)** 0.5 s, **(b)** 1 s, and **(c)** 1.5 s.

In contrast, with the center-slotted tool electrode, the debris particles are relatively evenly distributed at the bottom of the IEG (Fig. 7). At 0.5 s, most debris particles begin to move upward through the central slot pathway (Fig. 7(a)). As time increases to 1 s, some debris also migrates through the side gaps, though the velocity and quantity of debris particles are significantly greater in the central slot pathway compared to the side gaps (Fig. 7(b)). By 1.5 s, it is evident that the debris moves toward the micro-hole outlet through the central slot pathway (Fig. 7(c)). However, with the solid cylindrical tool electrode, at 1.5 s, a significant amount of debris remains trapped within the IEG (Fig. 6(c)). Additionally, the pressure gradient in the center-slotted tool electrode is notably higher (Fig. 5). As expressed by Eqs. (8)–(9), compared to the solid cylindrical tool, debris is removed from the IEG more rapidly with the center-slotted tool electrode (Figs. 6 and 7). Furthermore, as shown in Fig. 7(c), the debris is more

uniformly distributed at the bottom of the IEG, with a lower concentration than that observed under the cylindrical electrode condition. This indicates that most of the debris has either been evacuated or is actively being removed through the central slot pathway. Additionally, the center slot helps mitigate debris accumulation in the central gap caused by the secondary flow effect.This further demonstrates that the proposed self-flushing technique effectively utilizes the secondary flow effect to overcome debris evacuation challenges in deep-hole machining. It is anticipated that the center-slotted tool electrode can significantly enhance debris removal from the IEG, thereby offering the potential to process large aspect ratio (AR) micro-holes. To verify the simulation model, detailed experiments were conducted, and the results are reported in the following section.

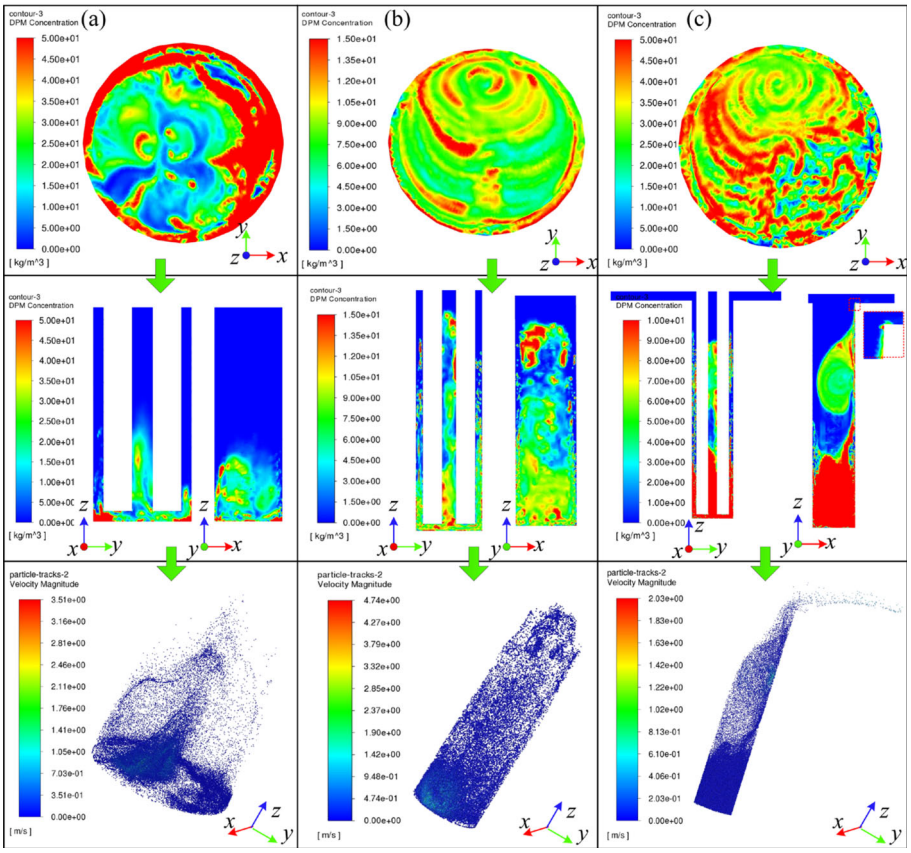

Fig. 7. The debris distribution in the center slotted tool electrode with different times: **(a)** 0.5 s, **(b)** 1 s, and **(c)** 1.5 s.

4 Experimental procedures

4.1 Materials

For all experimentation, they were conducted on the micro-electrical discharge machine (SX-200hpm, Sarix). In this study, the workpiece material was a titanium alloy (Ti6Al4V) with dimensions of 70×40×10 mm, the tool electrode material was a tungsten carbide (WC) rod and working liquid medium was hydrocarbon oil. Furthermore, the schematic of the center slotted tool electrode fabrication process is shown in Fig. 8. It can be seen that a 304-stainless steel sheet (i.e., it dimensions for length, height and thickness are 60 mm, 30 mm and 20 μm.) was fixed on the machine table and used to micro-EDM slotted the solid tool. In the tool fabrication process, the voltage was 100 V, the peak current 2.31 A, the frequency 10 kHz, the pulse width 20 μs, and the spindle speed 0 rpm, respectively. The working medium was hydrocarbon oil, while 304-stainless steel sheet as the negative, and the tool electrode as the positive. After the feed was completed, the tool electrode was slotted, and the WEDG module was then used to process the center slotted tool electrode to the required diameter (Fig. 8(b)). ~~Furthermore, the fabrication of shaped tool electrodes with diameters less than 200 μm is also relatively little challenge compared to other shaped tool electrodes.~~

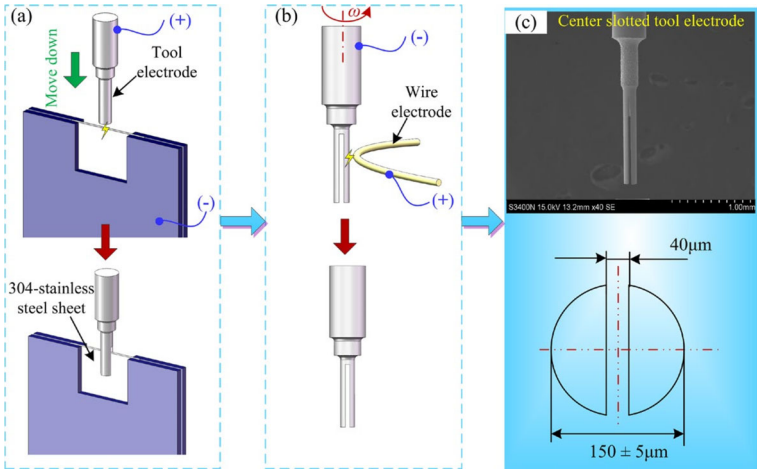

Fig. 8. Diagram of the slotted tool electrode fabrication: **(a)** slotted process, **(b)** electrode gridding by

WEDG, and **(c)** actual center slotted tool electrode.

4.2 Methodology

The main purpose of this investigation is focused on using the new self-flushing technique to increase the debris removal in the IEG central areas and understand its exhaustion mechanisms, subsequently enabling a large AR blind micro-hole to be processed. The present study compares the machining performance (i.e., machining efficiency, tool electrode wear and machining depth) of the center slotted tool electrode with the solid cylindrical electrode. Furthermore, the effects of slot position and width of the slotted tool electrode, pulse parameters, and rotation speed on machining performance were also studied. Each experiment repeated 5 times, and the detailed conditions were listed in Table 2. Finally, fabricating a micro-hole with a large AR using this new self-flushing technique further demonstrates the feasibility for increasing the micro-EDM performance.

Table 2. Processing conditions for the experiment investigation.

Parameters	Value
Voltage (V)	90, 100, 110, 120, 130
Frequency (kHz)	100
Pulse width (μs)	1, 2.5, 4, 5.5, 7
Rotation speed (rpm)	100, 200, 300, 400, 500
Peak current (A)	1.36
Tool electrode diameter (μm)	150
Slotted width (μm)	30, 40, 50

The workpiece was cleaned with an ethanol solution for 5 minutes both prior to and after the micro EDM drilling. After washing, the specimens are drying and then tested. To examine the cross-sectional appearance, the micro-holes were cut along the cross-section by wire-EDM process. Furthermore,

342 microscopic structures were analyzed and observed using SEM and EDS. A similar observation process
343 was also performed for the tool electrodes.
344
345 **5 Results and discussion**
346 **5.1 Comparison of the solid cylindrical and center slotted tool electrode**
347 In general, the frequent abnormal discharges due to the bubble and debris accumulation leads to a
348 decrease in the drilling feed rate, increase in tool wear, and limits the drilling depth [31]. To highlight the
349 advantages of the center slotted tool electrode with regard to machining efficiency, tool electrode wear
350 and depth of machining, a comparison study has been carried out. Micro-holes were fabricated with
351 different tool electrodes, the micro-hole depth is 0.5, 0.75, 1, 1.25, 1.5 mm. The voltage was 110 V, the
352 peak current 1.36 A, the frequency 100 kHz, the pulse width 4 μs, the spindle speed 500 rpm, and the
353 slot width 40 μm. Fig. 9(a) shows that both tool electrodes had an increase in machining time with the
354 intended micro-hole depth. However, machining time for the center slotted tool electrode was less than
355 the solid cylindrical tool electrode. In particular, after machining a depth for 1 mm, there is a significant
356 difference in machining time. For instance, when machining an intended micro-hole depth of 1.5 mm,
357 the machining time for the slotted tool electrode is only about 15.5 min, while the solid cylindrical tool
358 requires more than 50.4 min. That is to say, the center slotted tool electrode has a much better machining
359 efficiency than the solid cylindrical tool electrode.

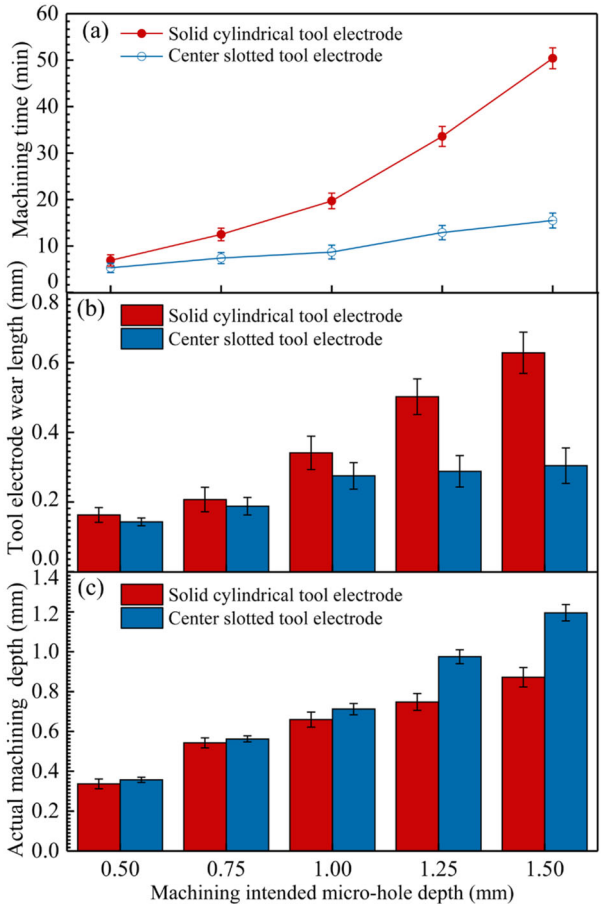

Fig. 9. The effect of the different tool electrode: **(a)** machining time, **(b)** tool electrode wear, and **(c)** actual machining depth.

Fig. 9(b) shows that the tool electrode wear of the center slot tool electrode is less than the solid cylindrical tool electrode. This change becomes more apparent with increasing micro-hole depth. For instance, when the intended micro-hole depth is 1.5 mm, the tool electrode wear length of the solid cylindrical tool electrode is 0.628 mm, whereas the center slotted tool electrode is only 0.304 mm. The larger tool electrode wear length means that more severe the tool electrode wear occurred. As discussed earlier, the insufficient debris removal frequently leads to unusual discharges and short circuits in the micro-EDM. Consequently, this results in increasing the tool electrode wear [12]. This demonstrate that the self-flushing electrode has a greater capacity for debris removal than in the conventional solid cylindrical tool electrode. It also can be seen from Fig. 9(c), that the actual machining micro-hole depth

of center slotted tool electrode is larger than in the solid cylindrical tool electrode. For instance, when the intended depth is 1.5 mm, the actual machining micro-hole depth of center slotted tool electrode is about 1.195 mm, while the solid cylindrical tool electrode is only about 0.872 mm. It indicates that the center slotted tool electrode has the potential for increasing the AR of blind micro-holes under similar experimental conditions.

Fig. 10 shows the SEM pictures of the tool tip and hole section views. A visible cone is form in the central hole bottom and the tool tip is wear to form a cone-shaped concavity in the solid cylindrical tool (Fig. 10(a)). In comparison, a micro-hole without the cone and tool electrode tip without conical concavity was processed by using the center slotted tool electrode (Fig. 10(b)). This importance is because that the debris accumulates in a cone formation at the hole bottom central area [27]. On the other hand, such debris is hard to evacuate from the center region of IEG [18]. Thus, the discharge material removed interactions between the debris particles and the tool continued. As a result, a cone is formed and its complementary conic-concave emerges on the tool tip. It is envisaged that the self-flushing electrode can effectively remove the debris out from the IEG through the central slot pathway, eliminating the accumulated debris near the center of the IEG.

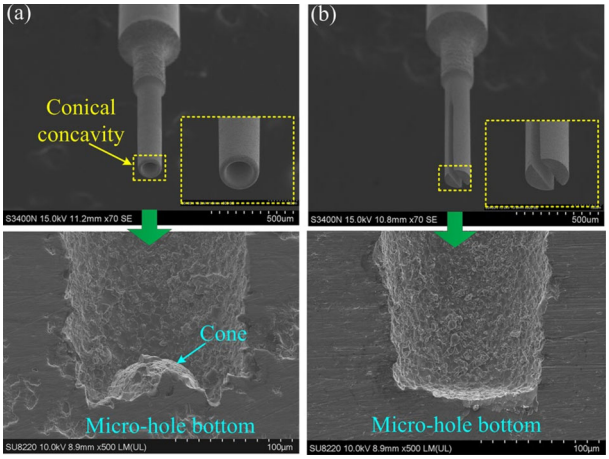

Fig. 10. The effect of different tool electrodes on micro-hole and tool electrode tip geometries: **(a)** solid cylindrical, and **(b)** center slotted tool electrode.

To further determine that the new self-flushing technique could effectively exhaust the debris from the IEG through the central slot pathway, Fig. 11 compares the SEM of the holes inner wall. As compared with the solid cylindrical electrode, only a small amount of debris is attached to the inner walls in the center slotted tool electrode (Fig. 11). These images reveal that the center slotted tool electrode has a better inner wall quality than that of the solid cylindrical tool electrode. It is also observed from Fig. 11 that more severe micro-hole side wall damage occurs in the solid cylindrical tool electrode than in the self-flushing electrode. It is well known that the debris particles are only removed through the side gap in the solid cylindrical tool electrode. There is no effective self-flushing effect using a solid cylindrical tool electrode [22]. Furthermore, since the side gap is too small, debris is frequently stuck in the side gap, and this evident from Fig. 11(a). As a result, the ineffective debris removal produces the excessive arcing and/or short circuiting in the side gap. In contrast, most of the debris can be removed through the central slot pathway of the self-flushing electrode, and hence less debris adhered to the inner wall of the micro-holes.

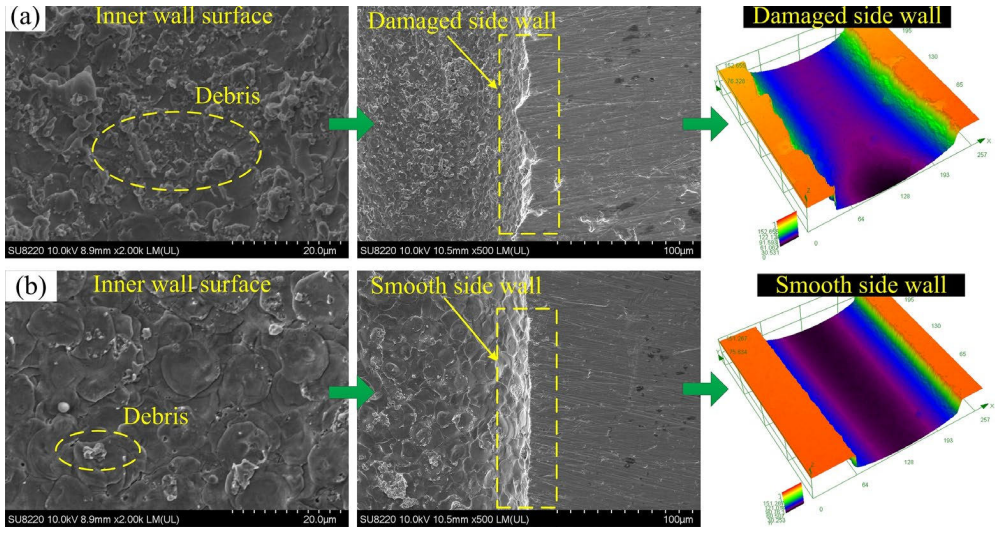

Fig. 11. The effect of different tool electrode on inner wall and profile of micro-hole: **(a)** solid cylindrical tool electrode, and **(b)** center slotted tool electrode.

Furthermore, the inner wall surface of the center channel has been investigated with SEM and EDS

analyses. Figs. 12a-b indicates the SEM images of the original inside surface of center slotted tool electrode. As can be seen, the inside wall of the original tool electrode has obvious electrical discharge melting micro-craters and re-melted material. Moreover, Fig. 12(c) indicates the EDS spectrum of the original tool inside wall. The C, O, W, Fe, and Co contents are approximately 62.8 At%, 7.35 At%, 21 At%, 0.25 At% and 8.6 At%, respectively. In comparison, Figs. 13a-b show the SEM pictures of the inside surface of the self-flushing tool electrode after drilling. There is a large number of debris particles on the inner wall surface of the center slot electrode (Fig. 13(b)). To further identify the debris material, inner wall surface of the center slot electrode was also examined by EDS analysis. In Fig. 13(c), the constituents of the Ti6Al4V workpiece material (Ti, Al, and V elements) can be observed on the inside wall of the center slot electrode. This experimental result confirms that the debris is removed through the central slot pathway of the center slotted tool electrode, which was very consistent with the simulation results.

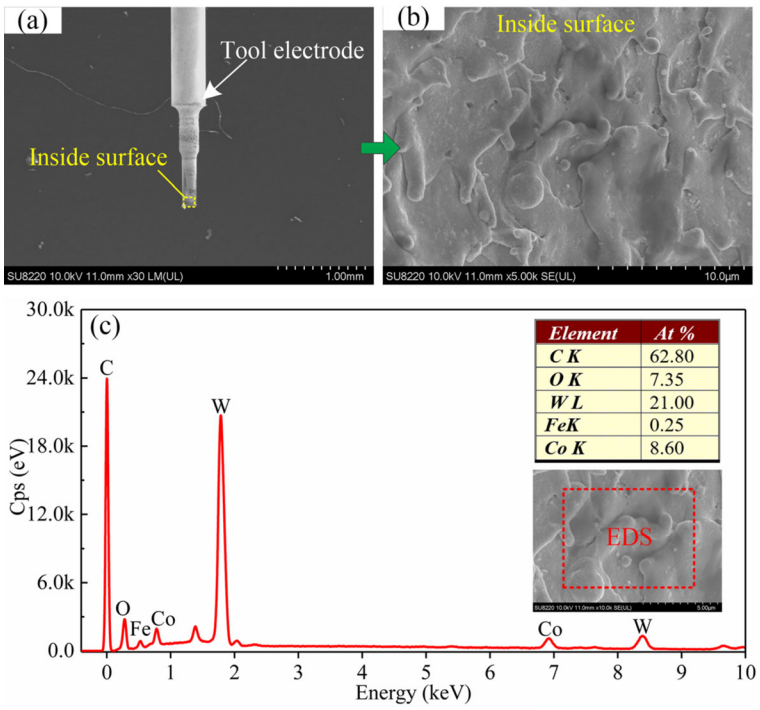

Fig. 12. (a) The SEM of original slotted tool electrode, **(b)** SEM images of the slotted tool electrode

inside surface, and **(c)** EDS analysis.

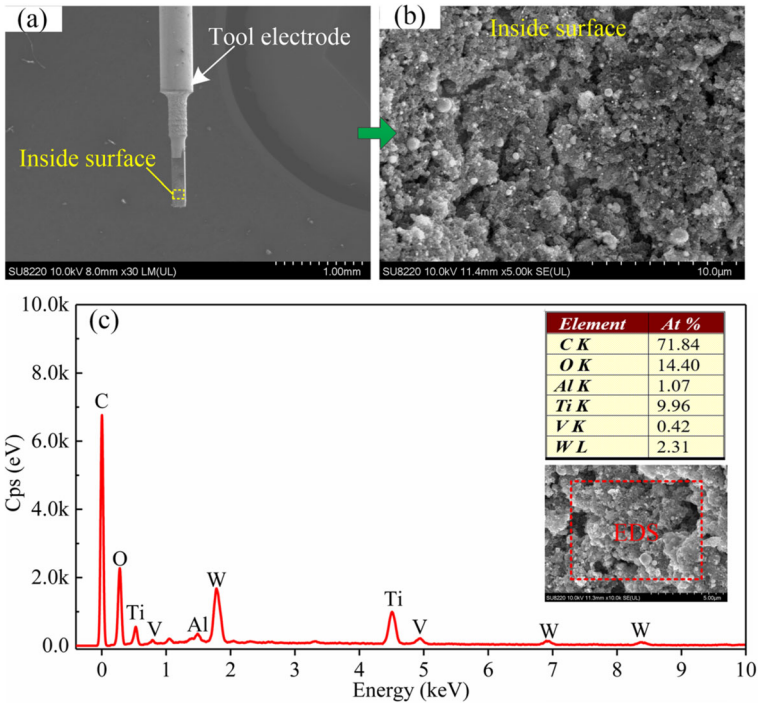

Fig. 13. (a) SEM of the center slotted tool electrode after machining, **(b)** SEM images of the slotted tool electrode inside surface, and **(c)** EDS analysis.

However, the IEG has a large number of bubbles and have a significant impact on debris removal in practical EDM drilling. Thus, to fully understand the self-flushing technique, a high-speed camera was applied to further studied the mechanism for the debris removal. As shown in Fig. 14(a), it can be observed that a small amount of bubbles exhaust from the side gap in the solid cylindrical tool electrode. Among the bubble expansion is the main cause of bubble movement and follows the debris removal from the IEG [13]. In general, a greater number evacuation of bubbles means the better the debris exhaustion efficiency [26]. However, due to the expansion of the bubbles, the size of the bubbles grows, resulting in a higher resistance to the bubbles movement. Thus, the debris is easier to re-solidify on the inner wall of micro-holes (Fig. 11(a)). The increased hole depth increases the difficulty of bubble evacuation, because the bubbles generated in the IEG have to resist greater pressure from the working liquid [32]. This is the reason why fewer and fewer bubbles escape from the micro hole (Fig. 14(a)). Moreover, without

436 additional flushing effect, a part of the bubbles is blocked in the hole wall, which affects the debris
437 removal [13]. Thus, frequent abnormal discharges and short circuits occur in the conventional EDM
438 drilling, resulting in a low EDM drilling performance (Fig. 9). In comparison, Fig. 14(b) shows that a
439 large number of bubbles remove from the slot pathway of the center slotted tool electrode. That is to say
440 that the center slotted tool electrode has a better debris evacuation efficiency than that of the solid
441 cylindrical tool electrode. Since the self-flushing effect is formed in the IEG by using the center slotted
442 electrode rotating. Although the bubble expansion and working liquid pressure caused resistance to its
443 movement in the case of center slotted tool electrode, this proposed self-flushing technique can provide
444 a driving flushing force to the bubbles. As a result, the working liquid is continuously flowing into the
445 IEG by self-flushing technique, thus both debris and bubbles are efficiently removed from the IEG,
446 causing an increase in EDM drilling performance. These results further proved that the debris can exhaust
447 from the slot pathway of the center slotted tool electrode, and the center slotted tool electrode has a better
448 debris evacuation efficiency than in the solid cylindrical tool electrode. These experimental results are
449 very well agreed with the simulation results.

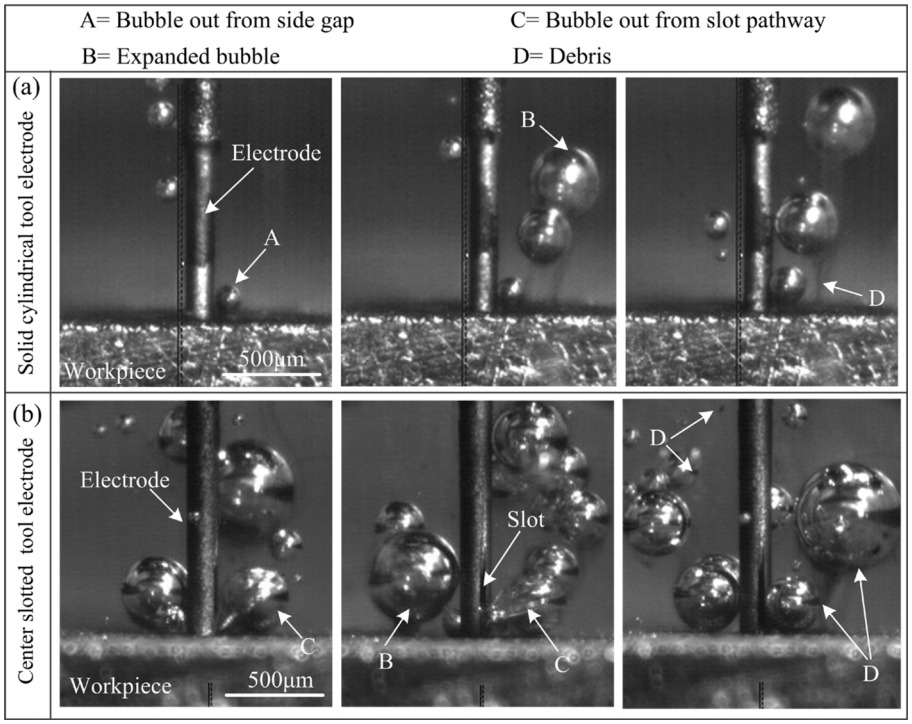

Fig. 14. High-speed photographs of the dynamic characteristics of bubbles in **(a)** solid cylindrical tool electrode, and **(b)** center slotted tool electrode.

5.2 Effect of slot position of the self-flushing electrode

As discussed earlier, the debris can effectively exit from the slot pathway of the center slotted tool electrode by using self-flushing effect. Furthermore, the slot position of slotted tool electrode also has a critical effect on the secondary fluid action. Thus, the slot position and width should be discussed. Fig.15 shows the different slot positions, such as edge, center, and offset slot. In this section, a voltage of 100 V, peak current 1.36 A, frequency of 100 kHz, pulse width of 4 μs, spindle speed of 500 rpm, and slot width of 40 μm were applied. Whilst the intended micro-hole depths were 1, 1.5, 2, 2.5, 3 mm.

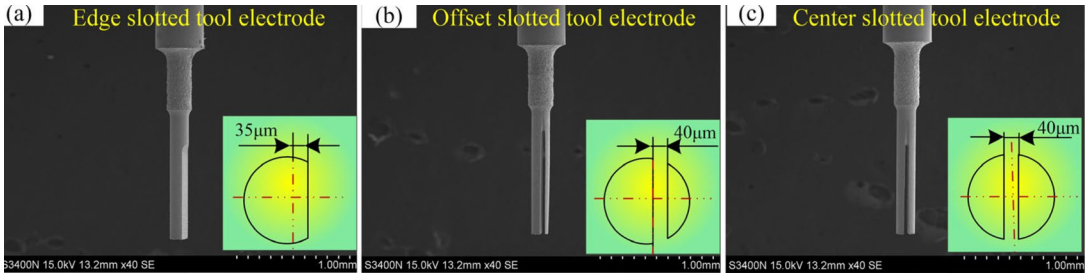

Fig. 15. The different slot position of slotted tool electrode: **(a)** edge, **(b)** offset, and **(c)** center.

As can been seen, both tool electrodes show an increase in machining time with micro-hole depth. However, the machining time for the offset slotted tool electrode is less than that of the center slot but larger than the edge slotted tool electrode under various intended micro-hole depths. For instance, when the intended micro-hole depth is 3 mm, the machining time of center slotted tool electrode is 34.5 min, the offset slotted tool electrode is 41.4 min and the edge slotted tool electrode is 45.5 min (Fig. 16(a)). Apparently, the center slotted tool electrode has higher machining efficiency than those of other electrodes (i.e. edge and offset tool electrode). Furthermore, the tool electrode wear length of the offset slotted tool electrode is less than for the center slot but larger than the edge slotted tool electrode under various intended micro-hole depths (Fig. 16(b)). Similarly, the actual machining depth has the same trend, as shown in Fig. 16(c). For example, when the intended micro-hole depth is 3 mm, the actual machining depth of the center slotted tool electrode is 2.185 mm, the offset slotted electrode is 1.957 mm and the edge slotted electrode is 1.876 mm.

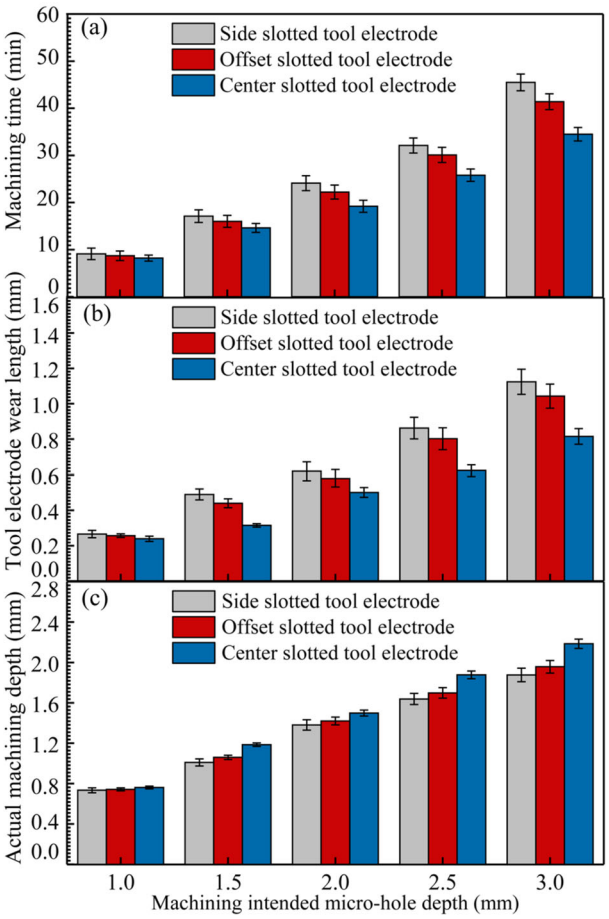

Fig. 16. The effect of the different slot positions of the slotted tool electrode: **(a)** machining time, **(b)** tool electrode wear, and **(c)** actual machining depth.

Fig. 17 indicates the SEM pictures of the section views of the micro-holes drilled with various slot position on the tool electrode. The debris accumulates at the micro-hole inside wall with different slot position of tool electrode conditions, however, especially for the edge slotted tool electrode, more debris accumulates gathered at the micro-hole inside wall (Fig. 17(a)). Although the edge slotted tool electrode has sufficient space to remove most of the debris from the side gaps, debris movement through the side gap, or accumulating with the micro-hole depth increases. Fig. 17(a) shows a magnified image of the micro-hole inside wall. Much debris accumulates at the inside surface of the micro-hole. As can be seen form Fig. 17(a), there is a slight cone in the central micro-hole bottom (Fig. 17(a)). That is to say, the debris is hard to be removed from the center region of IEG in the case of edge slotted tool electrode. In

contrast, in the offset slotted tool electrode, the debris gathering in the holes inside surface is still severe (Fig. 17(b)). But in case of the center slotted tool electrode, little debris accumulates at the inner wall. These indicated that most of the debris can be exhausted from the center slot pathway and a micro-hole without cone is obtained (Fig. 17(c)). It can be concluded that the self-flushing tool electrode has a better drilling performance. The number of debris adhering to the hole inner wall is less in the case of center slotted tool electrode. In contrast, in the case of offset and edge slot positions, a large amount of debris adheres to the hole inner wall. This indicated that most of the debris can be exhausted from the center slot pathway, whereas a considerable amount of debris accumulates in the hole sidewalls in the case of the edge and offset slot electrodes. These may result in the formation of secondary spark discharges within the sidewall gap, resulting in discharge craters with different shapes and sizes. Furthermore, there may be a certain influence of the different slot positions on the size and shape of the discharge crater in the inner wall of the hole. As shown in Fig. 17, in the center slot position condition, the discharge crater size of the hole inner wall is larger than that of the edge and offset positions.

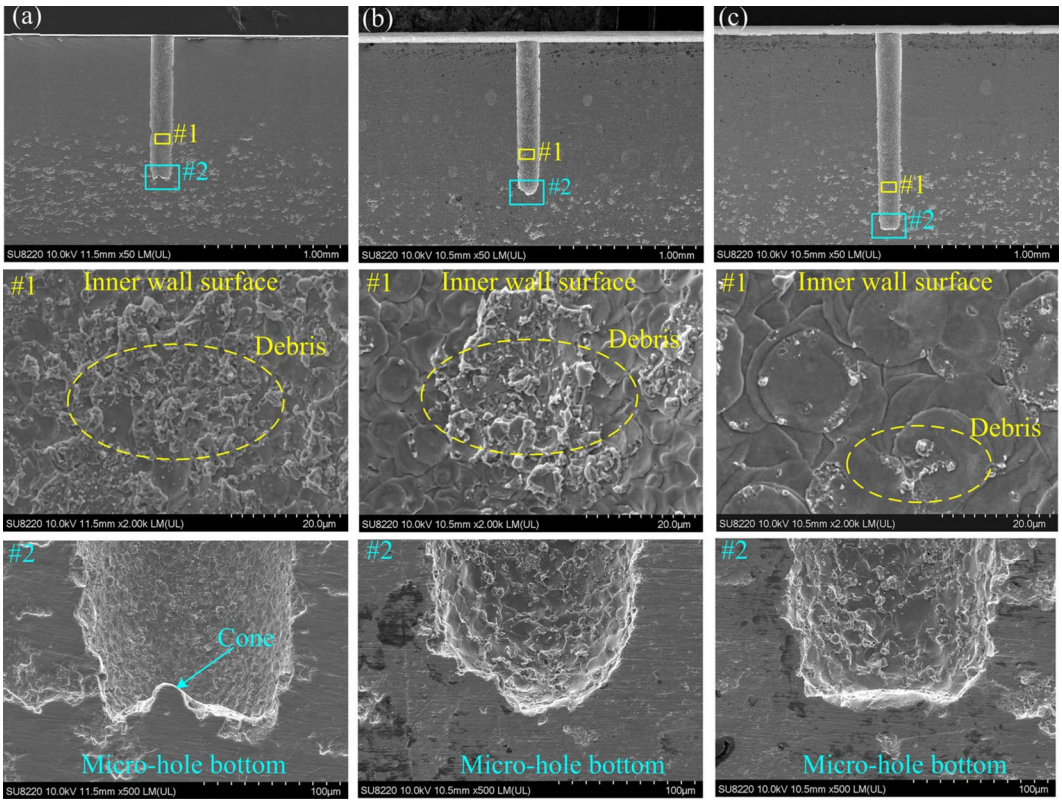

Fig. 17. SEM images of the section views of micro-holes under different slot positions of tool electrode conditions: **(a)** edge, **(b)** offset, and **(c)** center.

5.3 Effect of slot width of the self-flushing electrode

It should be noted that the slot width is also expected to have a critical effect on the machining performance. As a consequence, a comparative experiment was undertaken to study the effect of the slot width on the processing time, tool electrode wear and machining depth. In this study, a voltage of 100 V, peak current 1.36 A, frequency of 100 kHz, pulse width of 4 μs, spindle speed of 500 rpm, and an intended micro-hole depth is 2 mm were the reconditions. Whereas the slot width of the center slotted tool electrode was 30, 40 and 50 μm. As the slot width increasing, the machining time first decreased and then increased (Fig. 18(a-b)). Furthermore, as the slot width increased, the tool electrode wear length also decreased first and then increased. Although the secondary flow effect can allow the debris to exit

through the center slot pathway, the debris cannot be effectively removed due to the slot width being too small (i.e., 30 μm). As a result, a cone is forming at the bottom of the hole (Fig. 18(c)). Nevertheless, on further increasing the slot width, there was sufficient space remove most of the debris, but when the slot width was 50 μm, residue accumulated at the central area of the hole bottom (Fig. 18(d)). In comparison, a micro-hole bottom without a cone was avoided for a center slot width of 40 μm (Fig. 18(e)). As noticed, when the slot widths were 30μm and 50 μm, a cone and/or residue are formed at the central area of the hole bottom. Furthermore, which resulting in a serious tool electrode wear, significantly decreasing the drilling depth of the micro-hole. For instance, the machining depths for slot widths 30, 40 and 50 μm were 1.01 mm, 1.40 mm and 0.77 mm, respectively. Thus, the center slotted tool electrodes with a slot width of 40 μm are preferred for fabricating micro-holes with a high AR.

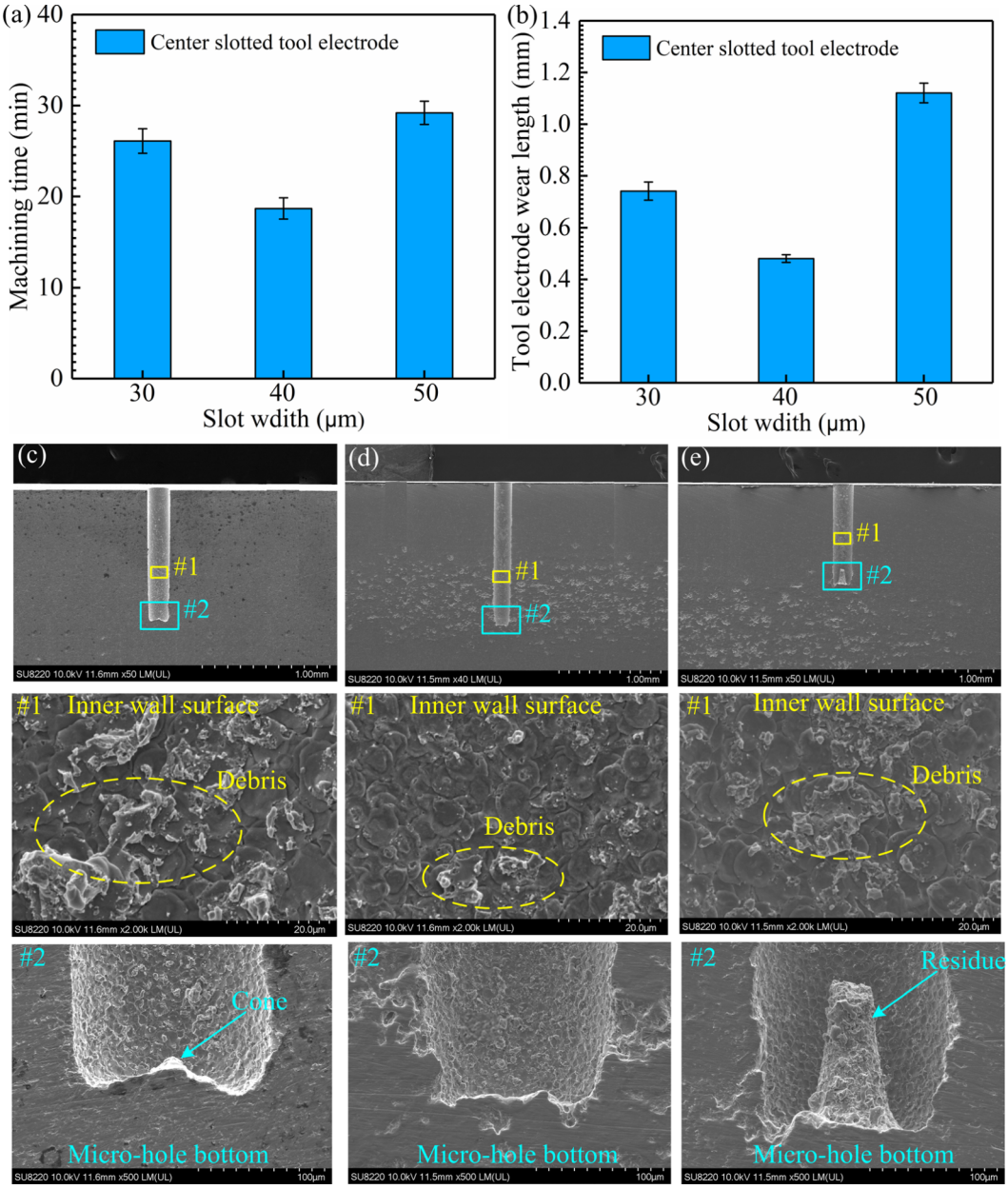

Fig. 18. The effect of slot width of tool electrode on **(a)** machining time, **(b)** tool electrode wear, and **(c-e)** SEM images of the section views of micro-holes with slot width is 30, 40, 50, respectively.

5.4. Effect of the tool electrode rotation speed

As discussed earlier, the tool electrode rotational speed also plays a critical role in the secondary fluid and self-flushing effect, however, the current micro-EDM machine (SX-200hpm, Sarix) has varying spindle in the range 0–500 rpm. Thus, the effect of various tool rotation velocity (i.e. 100, 200, 300, 400

and 500 rpm) on the machining performance was investigated as reported in this section. Voltage of 110 V, peak current of 1.36 A, frequency of 100 kHz, pulse width of 4 μs, and the intended micro-hole depth of 2 mm were fixed. Fig. 19 shows that, as the increase of tool rotation velocity from 100 rpm to 500 rpm, the machining time and tool electrode wear length decreased from 32.8 min to 20.2 min, and 0.764 mm to 0.553 mm, respectively. Whereas the machining micro-hole depth increased from 1.649 mm to 1.946 mm. Although the center slotted tool electrode provided a large slot pathway for debris removal, the secondary flow effect was insufficient to efficiently remove debris under the low tool rotation speed condition (i.e. 100 rpm).

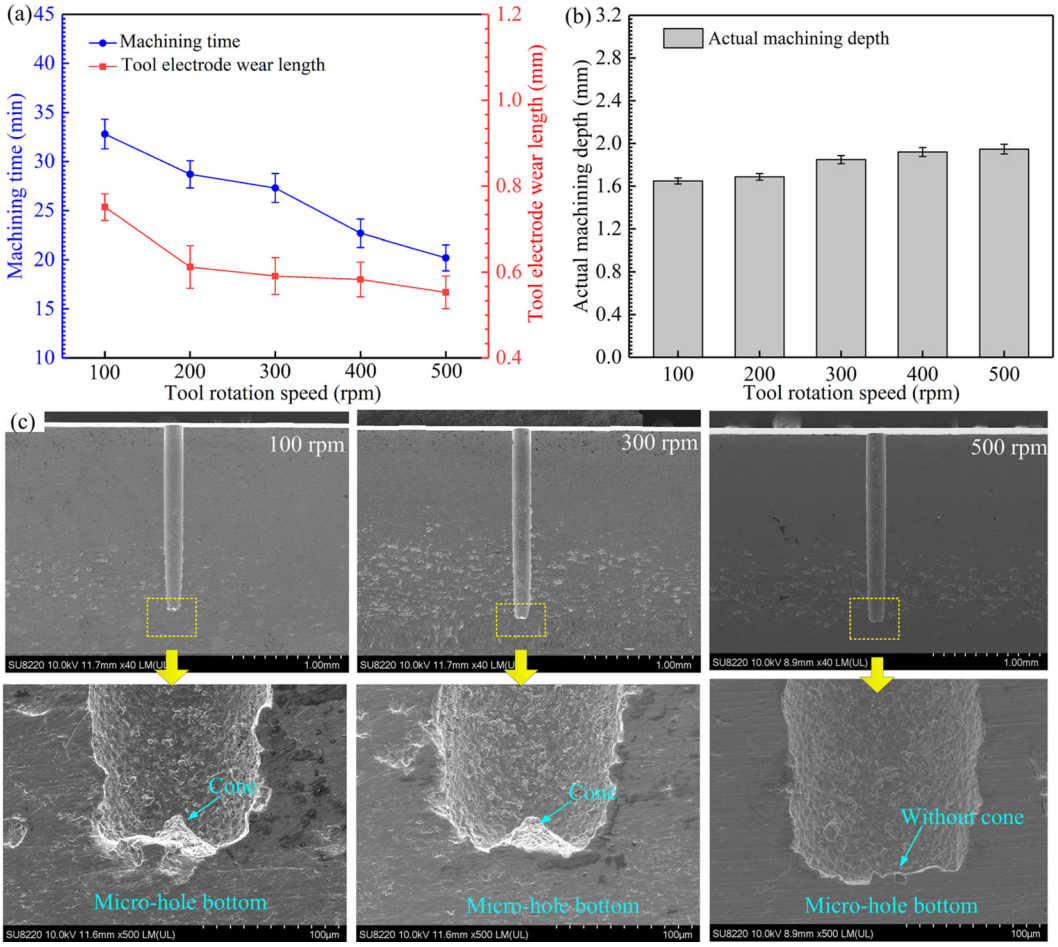

Fig. 19. The effect of tool electrode rotation speed on **(a)** machining time and tool electrode wear, **(b)** actual machining depth, and **(c)** the SEM images of the section views of micro-holes with various rotation speed.

However, it should be noted that the pressure difference (i.e., secondary flow effect) is proportional to the tool rotation speed, which means that the higher the tool rotation speed, the larger the secondary flow action. Apparently, further increased tool electrode rotation speed, resulting in an increasing debris exhaustion through the center slot pathway. Fig. 19(c) shows that when the rotation velocity is 100 rpm, the micro-hole bottom formed a cone. That is to say, the debris particles were hard to be evacuated from the center area of IEG with a low rotation speed, resulting in a forming a cone in the central area of micro-hole bottom [18]. In contrast, further increasing the rotation speed, the secondary flow effect, i.e., self-flushing effect is also increased, significantly improving the debris exhaustion. Thus, as the rotation speed increase, the cone of micro-hole bottom from to nearly flat (Fig. 19(c)). This is indicated that the rotation speed of 500 rpm was preferred for this process.

5.5 Effect of the pulse parameters

The pulse parameters (i.e., voltage and pulse width) also play a critical effect on the micro-EDM process. Thus, the effect of pulse voltage and pulse width on the machining process will be investigated. In this investigation, the remaining parameters were set: the pulse frequency of 100 kHz, peak current of 1.36 A, the slot width of 40 μm, the rotation speed of 500 rpm and the intended micro-hole depth of 2 mm. Furthermore, the pulse width and pulse frequency were maintained at 4 μs and 100 kHz, respectively. Micro-holes were fabricated with pulse voltage of 90, 100, 110, 120 and 130 V are shown in Fig. 20. When the pulse voltage increased from 90 V to 130 V, the processing time reduced from 26.2 min to 15.6 min, the tool electrode wear increased 0.543 to 1.462 mm, while the actual machining micro-hole depth reduced from 1.963 mm to 1.038 mm. In general, a greater the voltage, the higher the electrical melt and evaporative activity, and the better the machining efficiency. Nonetheless, the high pulse voltage

condition causes severe tool electrode wear, resulting in a decrease in the AR size. Furthermore, when using a low pulse voltage, the micro-holes had a good shape accuracy (Fig. 20(c)). However, further increase the pulse voltage led to damaging the side wall and a cone formed. Although low tool wear and better processing accuracy were found at the 90 V, fabrication of high AR micro-holes with a relatively high machining efficiency is the main target. Consequently, pulse voltage of 100 V is suitable for the self-flushing process.

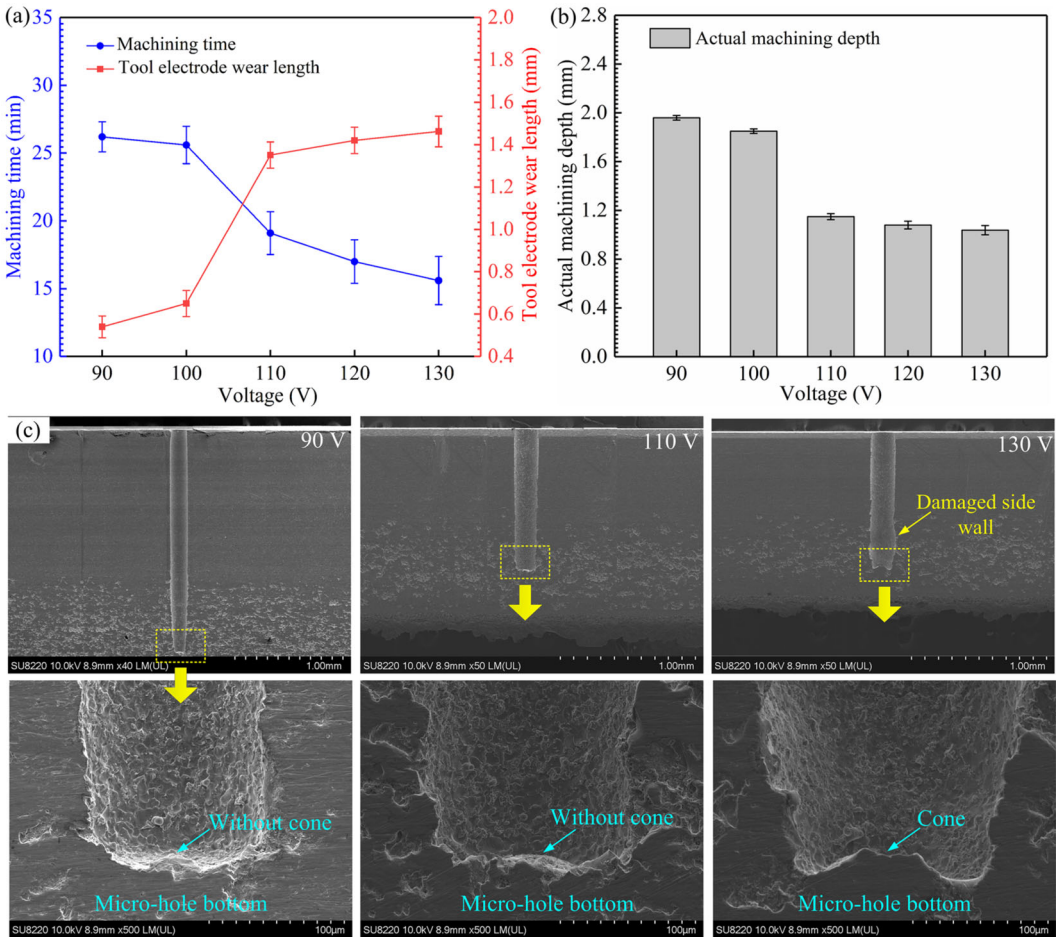

Fig. 20. The effect of pulse voltage on **(a)** machining time and tool electrode wear, **(b)** actual machining depth, and **(c)** the SEM images of the section views of micro-holes under various pulse voltage.

The effect of voltage is similar to that of pulse width, because larger voltages and/or pulse widths generate larger electrothermal energies inputs. Fig. 21 indicates the processing time, tool electrode wear length and actual machining depth of the micro-hole, while Fig. 21(c) compares the effect of pulse width

on the section views of the hole when processing at different pulse widths of 1, 2.5, 4, 5.5 and 7 μs. The frequency and pulse voltage were set at 100 kHz, and 100 V, respectively. It can be observed, with the pulse width increased from 1μs to 7 μs, the machining time decreased from 35.5 min to18.3 min, the tool electrode wear increased from 0.551 mm to 0.863 mm, while the actual machining micro-hole depth decreased from 1.945 mm to 1.554 mm. As shown in Fig. 21, a lower pulse width (i.e., 1μs and 4 μs) has a larger machining depth compared to a higher pulse width (i.e., 7μs). As discussed earlier, the self-flushing effect ensures sufficient de-ionization of the IEG during the subsequent pulse-on time, as most of the debris is effectively removed during the pulse-off time. However, it is important to note that with large pulse widths, the available pulse-off time for debris removal is reduced, which can limit the effectiveness of the self-flushing effect. In general, inefficient debris removal often leads to severe arcing and short circuits, resulting in increased tool electrode wear and a limitation in the achievable AR. Nevertheless, under large pulse conditions (e.g., 7 μs), there was no significant cone formation at the bottom of the micro-holes (Fig. 21(c)). This observation indicates that the self-flushing effect, generated at a tool electrode rotation speed of 500 rpm, successfully prevents debris from accumulating at the bottom of the hole. Consequently, a rotation speed of 500 rpm, a pulse voltage of 100 V, and a pulse width of 4 μs are identified as optimal parameters for fabricating large aspect ratio micro-holes with relatively high drilling efficiency.

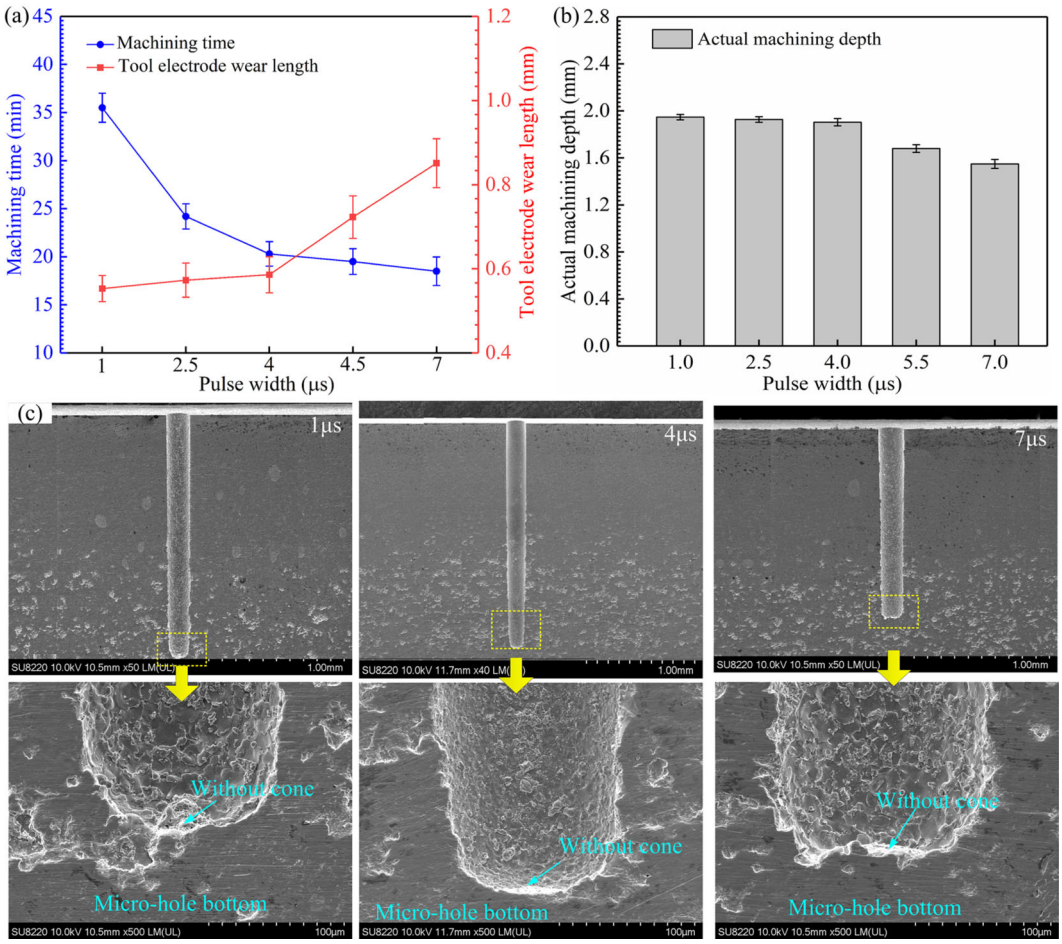

Fig. 21. The effect of pulse width on **(a)** machining time and tool electrode wear, (b) actual machining depth, and (c) the SEM images of the section views of micro-holes under various pulse widths.

6. Fabrication of micro-holes with a large AR

Based on above-mentioned experimental investigations, a large AR micro-hole was fabricated using the proposed self-flushing electrode with optimal parameters (i.e., pulse voltage of 100 V, peak current of 1.36 A, pulse frequency of 100 kHz, pulse width of 4 μs, rotation speed of 500 rpm, slot width of 40 μm). The fabrication time for the center slotted electrode is approximately 140 min for the length of the slot of 8 mm and average electrode diameter of 150 μm. Fig. 22 shows the image of the drilled blind micro-hole, in which the depth of the micro-hole is approximately 5.41 mm, and the entrance micro-hole diameter is about 197.3 μm. That is to say, a micro-hole with an AR of 27.42 was fabricated in Ti6Al4V

by the proposed self-flushing electrode. The processing time of drilling process is approximately 80 min, and the wear length of the electrode is 2.231 mm.It should be noted that Table 3 are also listed the results of micro-EDM in the present and existing studies on large AR micro-holes on Ti6Al4V alloys. Apparently, this is the highest AR reported so far in the literatures for Ti6Al4V alloy by micro-EDM. Furthermore, the holes inner/side wall surface are smoother and a relatively small amount of debris adhered to the inside wall (Figs. 22(a) and (c)). This further indicate that most of the debris exited through the central slot pathway of the self-flushing electrode, which is consistent well with the simulation result. Thus, it indicated that the proposed self-flushing electrode is a simple and effective method for drilling a large AR blind micro-hole.

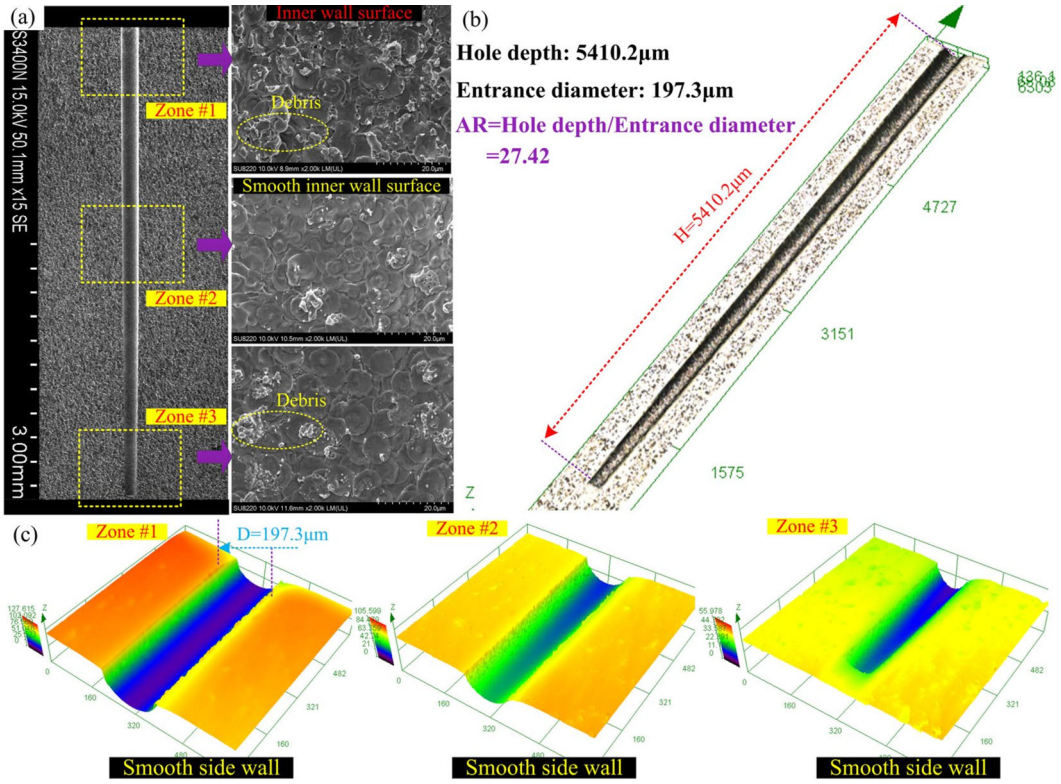

Fig. 22. (a) The SEM of the cross-section of the large AR micro-holes, **(b)** and **(c)** the 3D morphology of the cross-section of the large AR micro-holes.

Table 3. Comparison of the results of the present study with the existing literatures on micro-EDM of large AR blind micro-holes on Ti6Al4V alloys.

Authors	Workpiece materials	Depth of micro-hole (mm)	Micro-hole/tool dia. (μm)	Aspect ratio (AR)
Zhao et al. [16]	Titanium (Ti6Al4 V alloy)	3.2	200 (tool)	15
Plaza et al. [24]		6.81	661 (micro-hole)	10
Kumar et al. [25]		4.2	800 (tool)	7.5
Kumar et al. [26]		9.8	800 (tool)	12.25
Singh et al. [33]		10	574 (micro-hole)	17.42
Current investigation		5.41	197.3 (micro-hole)	27.42

7. Conclusions

This study proposed a novel self-flushing technique (i.e., center slotted tool electrode) to improve the debris removal in the IEG, fabricating a large AR blind micro-hole and with a good machining performance. From the combined analysis of simulations and experiments, the main conclusions below are drawn:

(1) Both the experiment and observation results were well supported the mechanism proposed for the debris removal. Using the center slotted tool electrode, the debris accumulated in the center IEG was effectively removed through the central slot pathway by the self-flushing effect.

(2) Compared to the solid cylindrical tool electrode, the processing performance is significantly improved with the center slotted tool electrode. The machining efficiency was increased about 73.1 %, and tool electrode wear was decreased about 62.5%.

(3) The slot position and width of the center slotted tool electrode and tool rotation speed play a critical role in the machining performances. The center slot, with a slot width of 40 μm is suitable for the

637 self-flushing effect. Further increasing the tool rotation speed, the self-flushing effect is increases
638 accordingly.
639 (4) By employing the optimal parameters, a micro-hole with a high AR of 27.42 (i.e., a depth of
640 5.41 mm, and entrance micro-hole diameter of 197.3 μm) was fabricated using the proposed self-flushing
641 technique, which is the highest AR reported so far in the literature for Ti6Al4V alloy using micro-EDM
642 drilling.
643 (5) The bubble expansion and working liquid pressure create resistance to bubble movement.
644 However, the proposed self-flushing technique generates a driving flushing force that facilitates the
645 movement of bubbles. As a result, the working liquid continuously flows into the IEG, enabling the
646 efficient removal of both debris and bubbles from the gap. This significantly enhances the EDM drilling
647 performance. In conclusion, the self-flushing technique demonstrates excellent potential and high
648 transferability for processing large AR blind micro-holes.
649
650 **CRediT authorship contribution statement**
651 **Zhixiang Zou**: Conceptualization, Methodology, Writing–original draft, Writing–review & editing.
652 **Zhijian Huang**: Investigation, Measurement. **Kangcheung Chan**: Formal analysis, Writing–review &
653 editing. **Taiman Yue:** Formal analysis. **Zhongning Guo:** Conceptualization, Methodology, Supervision,
654 Resources. **Jiangwen Liu:** Supervision, Resources.
655
656 **Declaration of competing interest**
657 The authors declare that they have no known competing financial interests or personal relationships that
658 could have appeared to influence the work reported in this paper.

Acknowledgments

The work described in this study was supported by the National Natural Science Foundation of China [Grant Nos. 52175387 and 52075104]. This work was also supported by the Natural Science Foundation of Guangdong Province, China [Grant No. 2024A1515011129], National Natural Science Foundation of China [Grant No. U22A2062] and Major research and development projects of Jiangxi Province [Grant No. 20223AAE02008].

Reference

[1] Leo Kumar, S. P., Jerald, J., Kumanan, S. & Prabakaran, R. (2014). A Review on Current Research Aspects in Tool-Based Micromachining Processes. *Materials and Manufacturing Processes*, 29, 1291-1337. https://doi.org/ 10.1080/10426914.2014.952037.

[2] Tiwary, A. P., Pradhan, B. B. & Bhattacharyya, B. (2019). Influence of Various Metal Powder Mixed Dielectric on Micro-EDM Characteristics of Ti-6Al-4V. *Materials and Manufacturing Processes*, 34, 1103-1119. https://doi.org/10.1080/10426914.2019.1628265

[3] Hasan, M., Zhao, J. W. & Jiang, Z. Y. (2017) A review of modern advancements in micro drilling techniques. *Journal of Manufacturing Processes*, 29, 343-375. https://doi.org/10.1016/j.jmapro.2017.08.006.

[4] Routio, M. & Saynatjoki, M. (1995). Tool wear and failure in the drilling of stainless steel. *Journal of Materials Processing Technology*, 52, 35-43. https://doi.org/10.1016/0924-0136(94)01441-3.

[5] Nasrollahi, V., Penchev, P., Batal, A., Le, H., Dimov, S. & Kim, K. (2020). Laser drilling with a top-hat beam of micro-scale high aspect ratio holes in silicon nitride. *Journal of Materials Processing Technology*, 281, 116636. https://doi.org/10.1016/j.jmatprotec.2020.116636.

[6] Zhang, Q. R., Luo, H. P. & Natsu, W. (2024). Parameter Identification of Equivalent Circuit for Pulsed Electrochemical Machining Based on Experimentally Obtained Current Waveforms[J]. International Journal of Precision Engineering and Manufacturing, 25,2491-2500. https://doi.org/10.1007/s12541-024-01112-6.

[7] Chen, X. L., Zhu, J. J., Xu, Z. Z. & Su, G. K. (2021). Modeling and experimental research on the evolution process of micro through-slit array generated with masked jet electrochemical machining. *Journal of Materials Processing Technology*, 298, 117304. https://doi.org/10.1016/j.jmatprotec.2021.117304.

[8] Fang, X. L., Wang, X. D., Wang, W., Qu, N. S. & Li, H. S. (2017). Electrochemical drilling of multiple small holes with optimized electrolyte dividing manifolds. *Journal of Materials Processing Technology*, 247, 40-47. https://doi.org/10.1016/j.jmatprotec.2017.04.013.

[9] Prakash, V., Kumar, P., Singh, P. K., Hussain, M., Das, A. K. & Chattopadhyaya, S. (2017). Micro-electrical discharge machining of difficult-to-machine materials: a review. *Proceedings of the Institution of Mechanical Engineers, Part B: Journal of Engineering Manufacture*, 233, 339-370. https://doi.org/10.1177/0954405417718591.

[10] Kumar, R., Agrawal, P. K. & Singh, I. (2018). Fabrication of micro holes in CFRP laminates using EDM. *Journal of Manufacturing Processes*, 31, 859-866. https://doi.org/10.1016/j.jmapro.2018.01.011.

[11] Gong, S.R., Wang, H., He, X. L., Wang, Z.L. & Wang, Y.K. (2023). One Step Fabrication of Micro-hole on SiCp/Al Cambered Surface by Micro-EDM and Mechanical-reaming Combined Machining *International Journal of Precision Engineering and Manufacturing-Green Technology*, 10: 891–903. https://doi.org/10.1007/s40684-022-00474-4.

[12] Jaber, A. Q., Ahmad, S., Ziout, A., Aiman, Z., Abdel-Hamid, I. M., Mustufa, H. A. & Ahmed, E. (2019). Advanced Electric Discharge Machining of Stainless Steels: Assessment of the State of the Art, Gaps and Future Prospect. *Materials*, 12(6), 907. https://doi.org/10.3390/ma12060907.

[13] Wang, J., Han, F. Z. (2014). Simulation model of debris and bubble movement in consecutive-pulse discharge of electrical discharge machining. *International Journal of Machine Tools & Manufacture*, 77, 56-65. http://dx.doi.org/10.1016/j.ijmachtools.2013.10.007.

[14] Wang, J., Han, F. Z. (2014). Simulation model of debris and bubble movement in electrode jump of electrical discharge machining. *International Journal of Advanced Manufacturing Technology*, 74, 591-598.

[15] Zhang, P., Yin, Z., Yu, M. X., Tao, D. Y., Yu, D. G., Zhang, Q. J. & Li, Hua. (2024). Investigating mechanisms of debris removal in ultrasonic vibration-assisted EDM drilling. *International Journal of Mechanical Sciences*, 279, 109486. https://doi.org/10.1016/j.ijmecsci.2024.109486.

[16] Zhao, W. S., Wang, Z. L., Di, S.C., Chi, G. X. & Wei, H. Y. (2002). Ultrasonic and electric discharge machining to deep and small hole on titanium alloy. *Journal of Materials Processing Technology*, 120, 101-106. https://doi.org/10.1016/S0924-0136(01)01149-9.

[17] Li, Z. K., Tang, J. J. & Bai, J. C. (2020) A novel micro-EDM method to improve microhole machining performances using ultrasonic circular vibration (UCV) electrode. *International Journal of Mechanical Sciences*, 175, 105574. https://doi.org/10.1016/j.ijmecsci.2020.105574.

[18] Ichikawa, T. & Natsu, W. (2013). Investigation of Machining Characteristics of Micro-EDM with Ultrasonically Vibrated Machining Fluid under Ultra-small Discharge Energy. *International Journal of Electrical Machining*, 18, 1-7. https://doi.org/10.2526/ijem.18.1.

[19] Ichikawa, T. & Natsu, W. (2013). Realization of Micro-EDM under Ultra-Small Discharge Energy

725 by Applying Ultrasonic Vibration to Machining Fluid. *Procedia CIRP*, 6, 326-331.
726 https://doi.org/10.1016/j.procir.2013.03.094.
727 [20] Bamberg, E. & Heamawatanachai, S. (2009). Orbital electrode actuation to improve efficiency of
728 drilling micro-holes by micro-EDM. *Journal of Materials Processing Technology*, 209, 1826-1834.
729 https://doi.org/10.1016/j.jmatprotec.2008.04.044.
730 [21] Yu, Z. Y., Zhang, Y., Li, J. J., Zhao, L. F. & Guo, D. (2009). High aspect ratio micro-hole drilling
731 aided with ultrasonic vibration and planetary movement of electrode by micro-EDM. *CIRP Annals-*
732 *manufacturing Technology*, 58, 213-216. https://doi.org/10.1016/j.cirp.2009.03.111.
733 [22] Li, G. D., Natsu, W. & Yu, Z. Y. (2019). Study on quantitative estimation of bubble behavior in
734 micro hole drilling with EDM. *International Journal of Machine Tools and Manufacture*, 146,
735 103437. https://doi.org/10.1016/j.ijmachtools.2019.103437.
736 [23] Li, G. D. & Natsu, W. (2020). Realization of micro EDM drilling with high machining speed and
737 accuracy by using mist deionized water jet. *Precision Engineering*, 61, 136-146.
738 https://doi.org/10.1016/j.precisioneng.2019.09.016.
739 [24] Plaza, S., Sanchez, J. A., Perez, E., Gil, R., Izquierdo, B., Ortega, N. & Pombo, I. (2014).
740 Experimental study on micro EDM-drilling of Ti6Al4V using helical electrode. *Precision*
741 *Engineering*, 38, 821-828. https://doi.org/10.1016/j.precisioneng.2014.04.010.
742 [25] Kumar, R. & Singh, I. (2018). Productivity improvement of micro EDM process by improvised tool.
743 *Precision Engineering*, 51, 529-535. https://doi.org/10.1016/j.precisioneng.2017.10.008.
744 [26] Kumar, R. & Singh, I. (2019). A modified electrode design for improving process performance of
745 electric discharge drilling. *Journal of Materials Processing Technology*, 264, 211-219.
746 https://doi.org/10.1016/j.jmatprotec.2018.09.014.

[27] Ekmekci, B. & Sayar, A. (2013). Debris and consequences in micro electric discharge machining of micro-holes. *International Journal of Machine Tools and Manufacture*, 65, 58-67. https://doi.org/10.1016/j.ijmachtools.2012.10.003.

[28] Einstein, A. (1926). Die Ursache der Manderbildung der Flulufe und des sogenannten Baerschen Gesetze. *Naturwissenschaften*, 14, 223-224. https://doi.org/10.1007/BF01510300.

[29] Zou, Z. X., Zhang, X. Y., Chan, K. C., Yue, T. M., Guo, Z. N., Wen, C. & Liu, J. W. (2023). An Analysis of the Uneven Tool Electrode Wear Mechanism in the Micro-electrical Discharge Machining Process. *International Journal of Precision Engineering and Manufacturing-Green Technology*, 10, 1-17. https://doi.org/10.1007/s40684-022-00499-9.

[30] Mastud, S. A., Kothari, N. S., Singh, R. K. & Joshi, S. S. (2014). Modeling debris motion in vibration assisted reverse micro electrical discharge machining process (R-MEDM). *Journal of Microelectromechanical Systems*, 24(3), 661–76. https://doi.org/10.1109/JMEMS.2014.2343227.

[31] Chen, Y., Mi, D. & Natsu, W. (2024). A Method to Enhance the Depth-to-Diameter Ratio of Micro-Holes Drilled with EDM Using the Pressure Difference Created at the Hole Entrance. *International Journal of Precision Engineering and Manufacturing.* https://doi.org/10.1007/s12541-024-01152-y.

[32] Li, G. D., Natsu, Wataru., Yang, J. F. & Yu, Z. Y. (2022). Bubble flushing effect in micro EDM drilling and its relation with debris. *Journal of Materials Processing Technology*, 305, 117590. https://doi.org/10.1016/j.jmatprotec.2022.117590.

[33] Singh, R., Dvivedi, A. & Kumar, P. (2020). EDM of high aspect ratio micro-holes on Ti-6Al-4V alloy by synchronizing energy interactions. *Materials and Manufacturing Processes*, 35, 1-16. https://doi.org/ 10.1080/10426914.2020.1762207.

Biography

Zhixiang Zou is an Associate Professor in School of Mechatronic Engineering, Guangdong Polytechnic Normal University. He received his Ph.D. in the State Key Laboratory of Precision Electronic Manufacturing Technology and Equipment of Guangdong University of Technology. He was a research assistant at the Department of Industrial and Systems Engineering of The Hong Kong Polytechnic University. His research focuses on advanced manufacturing technology and green precision engineering.

Zhijian Huang is a Master's candidate in Electromechanical Engineering, Guangdong University of Technology. His research focuses on the non-traditional machining.

Kangcheung Chan is Chair Professor of Manufacturing Engineering, Head of the Department of Industrial and Systems Engineering and Associate Director of Research Institute for Advanced Manufacturing of The Hong Kong of Hong Kong Polytechnic University. His research areas include Advanced Manufacturing Technology, and Materials Engineering and Processing.

Taiman Yue was a professor in the Department of Industrial and Systems Engineering of the Hong Kong Polytechnic University. He received his Ph.D.from the University of Southampton (UK). His research focuses on advanced manufacturing technology and advanced engineering materials. He is a chartered engineer.

Zhongning Guo is a Professor in school of electromechanical engineering at Guangdong University of Technology. He received his Ph.D. in industrial and systems engineering department from the Hong Kong Polytechnic University. His research focuses on micro machining and non-traditional machining.

Jiangwen Liu is a Professor in the State Key Laboratory of Precision Electronic Manufacturing Technology and Equipment of Guangdong University of Technology. He received his Ph.D. in the

Department of Industrial and Systems Engineering from the Hong Kong Polytechnic University. His research areas include Advanced Manufacturing Technology and Surface Engineering.